NACA RM E57E15

NACA

RESEARCH MEMORANDUM

EXPLORATORY INVESTIGATION OF STATIC- AND BASE-PRESSURE INCREASES RESULTING FROM COMBUSTION OF ALUMINUM BOROHYDRIDE ADJACENT TO BODY OF REVOLUTION IN SUPERSONIC WIND TUNNEL

By John S. Serafini, Robert G. Dorsch, and Edward A. Fletcher

Lewis Flight Propulsion Laboratory
Cleveland, Ohio

NATIONAL ADVISORY COMMITTEE
FOR AERONAUTICS
WASHINGTON

October 2, 1957
Declassified April 15, 1958

NATIONAL ADVISORY COMMITTEE FOR AERONAUTICS

RESEARCH MEMORANDUM

EXPLORATORY INVESTIGATION OF STATIC- AND BASE-PRESSURE INCREASES RESULTING FROM COMBUSTION OF ALUMINUM BOROHYDRIDE ADJACENT TO BODY OF REVOLUTION IN SUPERSONIC WIND TUNNEL

By John S. Serafini, Robert G. Dorsch, and Edward A. Fletcher

4139

CJ-1

SUMMARY

Pressure distribution associated with the stable combustion of aluminum borohydride about a body of revolution (parabolic forebody, cylindrical afterbody) was experimentally investigated in a wind tunnel at a Mach number of 2.47 and a free-stream static pressure corresponding to a 55,000-foot altitude. Fuel was injected through four circumferential and equally-spaced fuel orifices which were stationed 10.5 inches upstream of the base of a body 21 inches long.

Pressure increases on the cylindrical and base surfaces of the model were measured. Combustion resulted in static-pressure increases of about 2.0 inches of mercury on the cylindrical surface of the model. Base-pressure increased from 1.37 inches prior to combustion to 4.98 inches of mercury during combustion. Since these results were obtained in a small wind tunnel, they may be subject to undetermined wind-tunnel effects. Resolution of the uncertainties would require similar tests in a large wind tunnel or in free flight. Calculations showed that considerable reduction or possibly even complete cancellation of the total drag of the body of revolution may be obtained if these large increases in base pressure, measured in a small wind tunnel, can be duplicated in a free-flight situation or comparable large wind-tunnel tests.

INTRODUCTION

The effect of a heat addition to a supersonic airstream adjacent to bounding surfaces has received considerable attention in recent years. The results of analytical studies of heat addition to supersonic flow are presented in references 1 to 5. Reference 3 presents a graphical method for obtaining the flow field in a two-dimensional supersonic stream to which heat is added. By using this graphical method, reference 4 shows that moderate heat addition adjacent to a supersonic two-dimensional wing results in increased lift and reduced drag.

It was demonstrated in reference 6 that stable combustion of aluminum borohydride occurred when the fuel was injected into the airstream adjacent to the top wall of a supersonic wind tunnel. Stable combustion was achieved without flameholding devices. The flameholding properties, afforded by the wind-tunnel wall and attendant boundary layer, were apparently sufficient. The combustion of aluminum borohydride in a supersonic wind tunnel produced an increase of 20 to 40 percent in static pressure along the tunnel wall (ref. 7). Experimental data are presented in reference 8 on the static-pressure increases resulting from the combustion of aluminum borohydride in the stream adjacent to a flat-plate model in a Mach 2.46 wind tunnel. Reference 8 also presents temperature and pressure data taken within the heated region. 4139

The purpose of the present investigation was to measure the static-pressure changes on the cylindrical and base surfaces produced by the combustion of aluminum borohydride in a region enveloping the afterbody of an axisymmetric body in a supersonic wind tunnel. Previous experiments in reducing base drag of bodies of revolution have consisted of either bleeding air into the base region (refs. 9 and 10), or burning (or adding heat) in the wake region downstream of the base. In reference 11, a pyrotechnic was used as a fuel, and in reference 12, the fuel used was hydrogen.

This exploratory study of the aerodynamic effects of the combustion about the body of revolution used essentially the same experimental techniques as those used in reference 8 for combustion in the supersonic stream adjacent to a flat plate. No attempts were made to vary the fuel-flow rate or to control or measure it with a high degree of accuracy; the determination of optimum fuel-flow rates was considered beyond the scope of the present study. Consequently, the results are not discussed in terms of the over-all efficiency of this heat addition and are not compared to the more conventional thrust-producing systems such as ramjets or rockets.

The results are presented for 12 steady-state combustion runs at a Mach number of 2.47 and a Reynolds number of approximately 8.0×10^6. Combustion and the associated flow disturbances are briefly described and illustrated with high-speed motion pictures. The investigation reported herein was done at the NACA Lewis laboratory.

SYMBOLS

C_p pressure coefficient $(p - p_o)/q_o$ where q_o is the free-stream dynamic pressure and is equal to $\gamma p_o M_o^2/2$

d maximum body diameter, 1.75 in.

l body length, 21 in.

M Mach number

p static pressure, in. of Hg

Re Reynolds number (based on free-stream conditions and body length)

t_c time interval during combustion measured from instant of ignition as seen in high-speed motion pictures, sec

z,r,φ cylindrical coordinate system (see sketch with table I)

γ ratio of specific heats, isentropic exponent

Subscripts:

b base conditions

c with combustion

o free-stream conditions

APPARATUS AND PROCEDURE

The apparatus consisted of a supersonic wind tunnel, model, transient and steady-state pressure instrumentation, fuel-injection system, and a retractable ignitor.

Wind Tunnel and Model

A 1- by 1-foot nonreturn-type wind tunnel operating at a Mach number of 2.47 was used in this investigation. Total temperature and pressure of approximately 100° F and 47.8 inches of mercury, respectively, were maintained during the combustion runs. The dew point was held at -55° F or lower. The model was positioned in the tunnel (fig. 1) so that the base of the model was 2 inches upstream of the center of the 11-inch-diameter windows; the windows were used for schlieren and other types of observation. This position of the model was chosen because, the model being longer than the window, the flow around the base was of greatest interest.

The model and sting support used in this investigation are shown in figure 2. The near-parabolic forebody of the model was 10.5 inches long. The cylindrical afterbody was also 10.5 inches long with a cylinder diameter of 1.75 inches. This model was studied in a previous aerodynamic investigation at a Mach number of 3.12 (ref. 13).

4139

CJ-1 back

Static-Pressure Instrumentation

Static-pressure instrumentation consisted of 21 static-pressure orifices on the surface and 10 static-pressure orifices on the base of the model (shown in table I). The static-pressure orifices were numbered to simplify the following discussion. Fast response was assured by making the static-pressure orifices 0.048 inch in diameter. Nonburning pressure data were measured with butyl-phthalate differential manometers. The model and tunnel-wall pressure changes resulting from combustion were measured by differential pressure transducers using fixed reference pressures. Reference 8 gives a more detailed description (including the response characteristics and calibration procedures) of the static-pressure instrumentation. Static calibrations of these instruments, performed prior to and after the entire series of combustion runs, indicated an accuracy within ±5 percent in the range of pressure changes measured.

4139

Photography

During combustion, high-speed (1400 to 4500 frames/sec) schlieren motion pictures were taken of the flow about the base region of the model. High-speed (1300 to 4200 frames/sec) black and white motion pictures of the flame (directly photographed) were taken with a camera trained on one of the flat schlieren mirrors. In addition, color motion pictures taken at comparable speeds were used in the direct-flame photography for some of the combustion runs. Timing markers were provided in order to determine the film speed.

Fuel Injection and Ignition

The main features of the fuel-injection system (fig. 3) were described in reference 8. The only significant differences were in arrangement of model fuel lines and orifices. The fuel lines from the injector to the model consisted of a 1/8-inch copper tube manifolded to four 1/16-inch Inconel tubes. The four Inconel fuel tubes were led through the sting and model to the fuel orifices; these orifices were evenly spaced around the model at a distance z of 10.5 inches (see table I). To minimize orifice plugging during combustion and to provide for easy cleaning after the combustion runs, the length of the fuel orifices was made smaller than the model wall thickness, shown in figure 4.

Prior to fuel injection, the fuel lines leading to the model were continually flushed with a low-pressure helium flow. Fuel charges of 25 to 28 cubic centimeters of aluminum borohydride were injected under helium pressure for periods of 2.0 to 3.8 seconds. The helium injection pressure was maintained at 50 pounds per square inch gage except in runs 1 and 2 (table II) where a higher helium pressure (100 lb/sq in.) was used

to prevent plugging. This plugging resulted from solids that formed by the reaction of the fuel with traces of foreign materials in the newly-installed fuel system of the model.

The fuel-flow rate in cubic centimeters per second was indirectly determined by dividing the volume of the fuel charge in the injector by the combustion time interval. The volume of fuel was measured when the injector was filled. The maximum error in the measurement of the fuel volume was estimated to be about ±1 cubic centimeter for the fuel volumes used. The duration of combustion was measured from the traces of the pressure-change data. This method of time measurement does not consider the fuel-flow duration prior to ignition. As in reference 8 the measured time intervals have been arbitrarily increased by 0.2 second to account for the preignition and post-flame periods of the fuel flow.

An electric-spark ignitor (fig. 1) was used to ensure consistent ignition of the fuel. The ignitor, a steel rod with a 1/4-inch diameter, yielded a 1-joule repeating capacitance spark at a rate of 5 sparks per second across a 1/8- to 3/16-inch gap. The rod was insulated from the tunnel wall and after extending about 1 inch into the tunnel angled toward the model to a position 1/4 inch upstream of the model base.

Once ignition occurred, the flame quickly travelled upstream to the fuel orifices and, in general, remained seated there until the fuel was expended. In this investigation, after ignition was established, the ignitor was retracted from the model to remove any possible effects it might have on the combustion region or on the adjacent model static pressures. The retraction was initiated by a photoswitch that sensed the combustion. The ignitor was retracted by rotating the rod 90° about the axis perpendicular to the side tunnel wall. After the burning stopped, the ignitor returned to its original or extended position.

RESULTS

Ignition and combustion of the fuel occurred in every run made with the body of revolution. The data for all these runs, numbered 1 to 12, are listed in table II. Good combustion is considered to have been obtained in eight runs (runs 2, 3, 4, 5, 7, 9, 11, and 12). Good combustion was relatively uniform, and intense burning occurred adjacent to the afterbody (surface and base) of the model resulting in significant changes in the static pressures for the entire model boundary of the combustion region. The results presented and discussed herein are mainly concerned with these eight good-combustion runs.

For the group of good combustion runs, the fuel-flow rates were 10.6 to 12.8 cubic centimeters per second, a variation of ±9 percent, which is within the estimated error of measurement. Although the

fuel-flow rates for the weak combustion runs were considerably lower, for completeness, the data obtained for these weak combustion runs (1, 6, 8, and 10) are included in table II. A limited discussion of the weak combustions runs is presented in appendix A. The aerodynamics of the body of revolution without combustion are presented in appendix B where they are also compared briefly with the aerodynamics of similar bodies of revolution (refs. 13, 14, 15, and 16).

The effect of combustion on the free-stream flow was noted by measuring the static-pressures along the wind-tunnel walls at a distance z of 3.5 and 9.5 inches. During combustion there were no pressure changes on the wind-tunnel walls at these stations.

Description of Burning and Associated Flow Phenomena

Although a study of the nature of the combustion itself was not the object of this investigation, certain general characteristics of the combustion were noted so that pressures measured on the model during combustion might be properly evaluated. The portion of the flow and model which was observed is shown in figure 5.

Visual observation revealed that combustion produced a very bright yellow-green flame in the good combustion runs; this flame was characteristic of the flames studied in previous work. In the good combustion runs, the flame had a maximum diameter of about 9 inches at or near the model base. Within an axial distance from 3 to 8 inches downstream of the model base, the visible flame gradually died out. Visual observation of the model and sting after completion of runs revealed that the ash patterns on the model surface about the four orifices were similar for all good combustion runs. Further downstream on the model surface and base, the ash was evenly distributed.

As noted from the motion-picture observations, upon ignition of the fuel the flame quickly propagated upstream to the fuel orifices and expanded radially until steady-burning was reached (in the mean-value sense). Both ignition and subsequent establishment of steady burning are presented and discussed in appendix C.

Typical examples of steady burning (run 9) are shown in figures 6 and 7. The two frames (directly photographed) in figure 6 show that during steady burning, the axial extent of the flame varies somewhat, but the downstream termination of the flame is always in view (within 6 to 8 in. downstream of the base). The maximum diametrical extent of the flame (8 to 9 in.) is also visible in the figure. This view of the combustion is one which looks slightly upstream of the perpendicular to the schlieren window.

Two schlieren motion-picture frames of run 9, shown in figure 7, present a picture of the flow and shock waves associated with the combustion. As described in reference 8, the steady-state burning is accompanied by an oblique shock wave just upstream of the fuel orifices. In figure 7, the flame shock wave after reflection by the tunnel walls is seen as the downstream set of oblique shock waves. The intersection of the flame shock waves with the schlieren windows may be faintly seen in figure 7 as curves which can be approximated by hyperbolas. The interaction of the reflected flame shock waves with the burning or heated region yields a shock-wave structure which does not easily afford a quantitative picture of the flow in the region of interest. However, the absence of strong- or normal-type shock waves in the region viewed by the schlieren is clearly evident in figure 7.

Axial and Meridional Static-Pressure Data Obtained During Combustion

Figure 8(a) presents two types of axial variation for the static-pressure increases obtained from the good combustion runs. The pressure-change data in this and subsequent figures is presented in terms of $(p_c - p)$ where p and p_c are the absolute static pressures in inches of mercury prior to and during combustion, respectively. The data for run 11 is an example of the smoothest axial variation of pressure change $(p_c - p)$. The data for run 12 is an example of the greatest variation of pressure change $(p_c - p)$ with axial distance z. In either case, the measured pressure change is less than 0.01 inch of mercury from static-pressure taps 2 to 6. This means that the combustion did not alter the flow about the model from the nose to a position within 1/2 inch upstream of the fuel orifice.

While the two sets of data downstream of the fuel orifice are not precisely similar, the average values of $(p_c - p)$ in this range of z are about the same. For run 11, the value of $(p_c - p)$ sharply increases from zero at a z distance of 10 inches to a measured peak value of 2.18 inches of mercury at a z distance of 11 inches. As z increases from the peak position, the values of $(p_c - p)$ first decrease to a minimum of 1.85 inches of mercury and then increase less rapidly to a level of about 2.10 inches of mercury. For run 12, the data indicates a peak value of 2.56 inches of mercury at a z of 12 inches and a minimum of 1.45 inches of mercury at a z of 14 inches. This minimum value is also the lowest value obtained in the eight good combustion runs.

Figure 8(b) presents the axial variation of the pressure-change $(p_c - p)$ for all of the good combustion runs. While the measured values of $(p_c - p)$ vary from 1.45 to 2.72 inches of mercury downstream of the

fuel orifices, the bulk of the data points lie in the range of $(p_c - p)$ from 1.8 to 2.2 inches of mercury. This indicates that, for any particular run and aft of the peak region, the pressure changes do not vary appreciably with the axial distance z. Also, the differences among the individual runs may be considered small.

Faired curves of the axial variation of p_c, which is the absolute static pressure on the model during combustion, are presented in figure 9 for the average of the good combustion runs along with runs 4 and 9, the minimum and maximum runs of the axial data, respectively. Also included in figure 9 is the nonburning axial pressure-distribution curve (obtained from the data presented and discussed in appendix B). The absolute pressures during combustion p_c are obtained by adding the pressure changes $(p_c - p)$ to the nonburning static pressure p. The values of p shown by the curve in figure 9 are calculated for a total pressure of 47.75 inches of mercury (average value of total pressure for all the good combustion runs). The static pressures resulting from combustion are about 70 percent greater than those without combustion.

The meridional variation of the pressure changes $(p_c - p)$ resulting from combustion is presented in figure 10. The data presented include only those good combustion runs for which the most complete sets of data points were obtained at the meridional stations. For a z distance of 17.5 inches (fig. 10(a)), the pressure changes for run 2 are virtually constant for the meridian angle φ from -90° to 90°. The slight asymmetry of the meridional pressure-change distribution for the other runs may result from slight inequalities in the fuel flows from the individual fuel orifices. In figure 10(b) at a z distance of 20.5 inches, the data is presented for φ from 0° to 90°. In general, the meridional variation appears to be about the same at this station. The data presented in figure 10 show that there is no significantly large meridional variation in the pressure changes resulting from combustion.

No effect of the fuel-flow rate on pressure changes could be obtained for the good combustion runs. For these eight good-combustion runs, their fuel-flow rates of 10.6 to 12.8 cubic centimeters per second may be represented by a single value of the fuel-flow rate if the indicated errors of measurement are taken into consideration. While considerably lower values of the fuel-flow rate were obtained for the weak-combustion runs (1, 6, 8, and 10), they are not useful in a study of the effect of fuel-flow rates on the static-pressure changes. The lower fuel-flow rates, presumably occurring because of poor or no fuel flow through one or several of the fuel orifices, resulted in the character of the combustion region being drastically changed from that of the good-combustion runs. For example, runs 8 and 10 with fuel-flow rates of 6.0 and 8.0 cubic centimeters per second, respectively, were essentially runs with combustion occurring only downstream of the model base (appendix B).

4139

CJ-2

Base-Pressure Data During Combustion

The most significant increase in pressure resulting from combustion occurred on the base of the model. The data obtained from the 10 base-pressure statics are plotted separately in figure 11 and also figure 12 simply for convenient presentation. The variation with the meridian angle φ from 0° to 90° is presented in plots (a) and (b) of figures 11 and 12 for r values of 0.63 and 0.81 inch, respectively. The (c) plots of figures 11 and 12 give the data at φ of 90° for r from -0.63 to 0.81 inch. For runs with ignitor retraction occurring, the base-pressure changes measured during combustion have been corrected for the slight change in base pressure resulting from ignitor retraction (see appendix B).

The pressure-change data for the base is presented in figure 11 for the eight good combustion runs. In this figure, the extreme values of $(p_c - p)$ are 3.47 and 3.90 inches of mercury, which is a variation of less than ±6 percent (based on the average of the extreme values). Comparing the average $(p_c - p)$ data for the four runs having high fuel-flow rates did not indicate even a slight trend with varying fuel-flow rate. For the good combustion runs, the base-pressure changes are relatively independent of any sort of grouping with the possible exception of run 9 which gave slightly higher values than the rest of the runs.

The average of the good combustion data and data without combustion is shown in figure 12 in terms of base pressures in inches of mercury absolute (for average total pressure of 47.75 in. of mercury). Figure 12 clearly shows the large magnitude of the base-pressure increase, as a result of the combustion reported herein. The average absolute pressure in the base during combustion is 4.98 inches of mercury as determined from the averaged data points in figure 12.

The base-pressure data for the four runs (1, 6, 8, and 10), which resulted in weak combustion presumably because of partially plugged fuel lines, is presented in appendix A.

DISCUSSION OF RESULTS

The combustion about the model in the 1- by 1-foot supersonic wind tunnel resulted in a region of flame at its maximum cross section about 8 to 9 inches in diameter. This fact, along with the substantial pressure increases on the base and along the model axis, suggests that the results be carefully inspected for the possible existence of wind-tunnel phenomena which may have affected the results quite significantly. If these wind-tunnel effects exist, then possibly the results reported herein cannot be duplicated in free flight.

Since it was not possible actually to observe the flow upstream of the schlieren window, an approximate picture of the flow in this upstream region was constructed by sketching in the flame and shock waves. This is done by using as references the places where the shock waves and flame not only originate, but also enter the combustion or heated region. The sketch is for a plane cross section, which includes the model centerline. This cross section is perpendicular to the wind-tunnel side walls and to the schlieren light path through the tunnel (φ, 0° or 180°).

Figure 13 presents a sketch of the flow about the entire model for run 9. The intersection of the three-dimensional shock waves with the cross section of the plane is shown as a solid line. The flame and heated regions are shown as a shaded area about the model afterbody. The portion of the flow under schlieren observation is denoted by a dashed line. The sketch does not show the nose and combustion shock waves entering the flame and heated region (shaded), because careful scrutiny of the schlieren motion-picture frames does not yield any certain evidence that the nose and combustion shock waves penetrated the combustion region. In figure 7, what may be taken as shock waves traversing the combustion and heated region may actually be shock waves existing outside of and adjacent to this region, which could consist of subsonic flow. The nature of the interaction of shock waves and the combustion region can be answered only by further research.

The schlieren motion-picture and pressure-change data along the model axis provide a definite answer on whether or not choking of the airflow occurred for the axial positions viewed with schlieren and also for the upstream positions. If, during combustion, choking of the flow did occur at these positions in the test section of the wind tunnel, then static-pressure increases on the model and wind-tunnel walls upstream of the combustion would have resulted. As discussed previously, the results do not show any static-pressure increases ahead of the combustion region on the model or wind-tunnel walls. In addition, none of the schlieren motion pictures show any normal-type shock waves moving to any position upstream of the schlieren window or existing within the region viewed. This holds from a time prior to ignition, and at all subsequent times including the period of steady burning.

The nonexistence of other wind-tunnel effects on the pressure-change results cannot be shown. The lack of any clear-cut picture of the flow or of any pressure or temperature data within the combustion or heated region does not allow a determination of the Mach-number distribution in this region. A knowledge of the Mach number in the region downstream of the base would be of particular importance. If an appreciably large subsonic region (see ref. 8) existed adjacent to the sting support, the pressure increases obtained on the model base and further upstream could have resulted, at least in part, from the pressure energy being fed in through this subsonic region from strong shocks. These shocks certainly may be assumed to exist further downstream in the wind tunnel.

4139

Even though the position and strength of these shocks in the wind tunnel are not known, the schlieren motion pictures do not indicate that any such shocks existed within the region viewed (7 to 8 in. downstream of the model base).

What effect the presence of the sting support had on the combustion is also not actually known. Since most of the visible flame occurs upstream of the sting support, it may be that the combustion was not greatly affected by the presence of the sting support. However, the base pressure may still be affected by the presence of the sting support because of the lowered Mach number (of unknown magnitude) occurring in the heated region.

The experimental work with the body of revolution and that with the 25-inch (extended) flat plate reported in reference 8 were carried out with similar objectives. In fact, both investigations were conducted in the same wind tunnel and at the same Mach number and static pressure. Also, the fuel amounts and times of injection were approximately the same. The combustion for the two models did not yield exactly the same results. The dissimilarities may have resulted in part from the fact that the combustion about the body of revolution resulted in a fairly axisymmetric region of flame, whereas the combustion adjacent to the flat plate resulted in a fairly two-dimensional region of flame.

The pressure changes resulting from combustion are of the same order of magnitude for both the body of revolution and the flat plate. The principal difference in the pressure-change data for the two models is the magnitude of the peak and minimum values which occurred downstream of the fuel orifices. For the body of revolution, the difference of the peak and minimum values was only 0.59 inch of mercury with the minimum pressure change being 1.79 inches of mercury for the average of the good combustion runs. In the case of the flat plate for similar quality data, the difference between the peak and minimum values was 2.15 inches of mercury. For both models, the pressure changes averaged over the length of the combustion region are about the same being 1.7 and 2.0 inches of mercury for the flat plate and body of revolution, respectively.

The large base-pressure increases (fig. 12) indicate considerable reductions in drag of the body of revolution. Appendix D presents calculations of the net axial forces acting on the model with and without combustion. An estimate of the skin-friction is also included in appendix D. At a free-stream static pressure of 2.93 inches of mercury and a Mach number of 2.47, the total drag of the model is 3.38 pounds. As a result of the greatly increased base pressure during combustion, summing the axial forces which act on the model results in a net thrust of 0.27 pound (when the average base pressure for all the good combustion runs is used). The reduction in drag is also appreciable for a weak combustion run during which burning occurred only downstream of the model base (run 10). In this case, the sum of the axial forces resulted in a drag of 0.30 pound.

4139

CJ-2 back

These significant drag reductions must be considered along with the preceding discussion on the possibilities of the wind-tunnel environment influencing the flow in the combustion region downstream of the base and, consequently, the base pressures during combustion. As remarked previously, if downstream of the model base a significant portion of the combustion region is subsonic, the wind-tunnel effects on the base-pressure increases may be of the first order. If this is the case, the previously mentioned reductions in drag would not be reproducible under free-flight conditions. In order to check this uncertainty, additional experimental work should be performed either in appropriate large-sized wind tunnels or in free flight.

4139

CONCLUDING REMARKS

Measurements were made of the pressure increases obtained from the combustion of aluminum borohydride about a body of revolution in a supersonic wind tunnel. This combustion, external and adjacent to the cylindrical and base surfaces of the afterbody, was stable and was readily maintained for the entire period of fuel flow (several seconds). On the cylindrical portion of the afterbody, the good combustion runs resulted in measured static pressures rises of about 2.0 inches of mercury; these pressure increases being approximately constant with respect to meridional variation. The base pressures were increased from 1.37 inches of mercury without combustion to an average of 4.98 inches of mercury for good combustion. Since these results were obtained in a small wind tunnel, they may be subject to quantitatively undetermined wind-tunnel effects. Calculations showed that considerable reduction or even complete cancellation of total drag of the body of revolution may be obtained if large increases in base pressures measured during combustion can be duplicated in a free-flight situation.

Further experimental work in a larger wind tunnel or in free flight should be performed to determine whether the pressure increases obtained were not only the result of the combustion, but also a function of wind-tunnel phenomena other than flow choking. In some of the further work, considerably longer burning times would also be desirable to determine what effects may or may not exist as the model surface temperatures attain steady-state or equilibrium values. Additional experiments should also be carried out which would allow a description of the burning region in terms of the pertinent thermodynamic and fluid-dynamic variables.

Lewis Flight Propulsion Laboratory
National Advisory Committee for Aeronautics
Cleveland, Ohio, May 20, 1957

APPENDIX A

BASE-PRESSURE DATA FOR WEAK COMBUSTION RUNS

Four runs (1, 6, 8, and 10) resulted in weak combustion presumably due to partially plugged fuel lines. This weak combustion resulted in smaller pressure increases along the body surface and base. Since combustion occurred only downstream of the base for runs 8 and 10, no pressure increases were noted upstream of the base for these runs. Of the weak combustion runs, only run 6 approached the surface- and base-pressure increases obtained for the good combustion runs.

The combustion for runs 1 and 6 is similar to that of the good combustion runs except that the diameter of the flame is smaller and its visible length is larger. Runs 8 and 10, having combustion only downstream of the base, are not similar to the good combustion runs.

The base-pressure changes during combustion are presented in figure 14 for the four weak combustion runs (1, 6, 8, and 10). For the data in figure 14, the $(p_c - p)$ values varied over a considerable range from 1.30 to 3.26 inches of mercury.

APPENDIX B

AERODYNAMICS WITHOUT COMBUSTION

Aerodynamic measurements of the model without combustion were necessary for analysis of the combustion data. Furthermore, these measurements can be compared with more complete aerodynamic experimental studies of bodies of revolution. The Reynolds numbers for the aerodynamic tests without combustion were changed from 6.7×10^6 to 10.9×10^6 by varying the tunnel stagnation pressure from 34.7 to 57.1 inches of mercury at a stagnation temperature of 53° F. This Reynolds number variation did not affect the measured pressure coefficients on either the model surface or on the model base. In order to determine the effect of the ignitor on the model pressures, data were obtained at two ignitor settings for a Reynolds number of 9.0×10^6. One ignitor setting was with the ignitor retracted from the model surface. The other was with the ignitor in the forward or extended position. The distance between ignitor and model at the extended ignitor position was approximately 1/8 to 3/16 inch. Slight variations within this range in the gap distance did not affect the pressures measured on the model surface and base.

A schlieren photograph of the flow about the rear portion of the model is presented in figure 5 for the ignitor retracted. The pressure distribution about the model without combustion is presented in figure 15 in terms of the pressure coefficient C_p. Coordinates of the static-pressure taps on the surface and base of the model are given in table I. Figure 15(a) presents the variation of C_p with the axial distance z along the body surface. Figure 15(b) presents the meridional variations of C_p at two axial stations. The data of figures 15(a) and (b) indicate that retracting the ignitor does not affect the model surface-pressure distribution. These data are also in general agreement with the data for the same model and Reynolds numbers at a Mach number of 3.12 (ref. 13).

The C_p distribution on the model base is given in figure 15(c). In this case, changing the ignitor setting does affect the base-pressure distribution. The pressure coefficients decrease as the ignitor is moved forward from the retracted to the extended position. In terms of pressure, the differences of the retracted and extended base-pressures range from 0.04 to 0.20 inch of mercury. These differences obtained with the ignitor settings are accounted for in the analysis and presentation of the combustion data.

A study of the schlieren photograph of figure 5 reveals that the nose shock wave reflected from the tunnel walls intersects the sting support at an approximate distance of 4/3 model diameters from the base

of the model. Prior to this investigation, the model was designed and used for a Mach number of 3.12 and a 1- by 1-foot wind-tunnel test section. In the present investigation at a Mach number of 2.47 and the same size test section, the reflected nose shock wave is closer than that usually considered desirable (see appendix B of ref. 14). However, the base-pressure data with the retracted ignitor are typical of data obtained in base-pressure studies (refs. 13 to 16). This is seen by comparing base-pressure coefficients, as in figure 16, which gives base-pressure coefficients as a function of Mach number. The base pressure in this investigation is in good agreement with the results of the references. For this investigation, the average C_p of -0.125 is obtained from figure 15(c).

The data in figure 16 are for cylindrical bases and include Reynolds numbers from 6.5×10^6 to 10×10^6 and body fineness ratios from 5 to 12. The values in figure 16 are for the cases where the transition to the turbulent boundary layer has presumably taken place on the body surface.

APPENDIX C

IGNITION AND ATTAINMENT OF STEADY BURNING

Figure 17, taken from the motion pictures of a typical good combustion run, shows the ignition and achievement of the steady burning of run 3. Figures 17(a) and (b) consist of the directly photographed and schlieren motion-picture frames, respectively. The time interval included in the series of selected single frames is from ignition to about 0.18 second after ignition. The time intervals (t_c) were referenced to the first frame in which flame appeared.

Thus, in figure 17(a), frame 1 gives the first evidence of illumination and shows the flame at a position slightly upstream of the ignitor and extending downstream of the model base. Frame 2 (t_c, 0.001 sec) shows a further upstream advance of the flame. In frame 3 (t_c, 0.003 sec) the combustion has apparently reached the fuel orifices. Frames 3 to 8 (fig. 17(b)) indicate the buildup of the combustion from a thin annulus of flame to a flared-out flame as in frames 7 and 8. The time of frame 8 is 0.179 second after burning started. Frames 7 and 8, typical of frames for subsequent times, represent steady-state combustion on the basis of visual observation and measured static-pressure changes. As steady-state combustion is reached, the length of the combustion region decreases so that the downstream limit of the visible combustion approaches the base region of the model. Also seen in frames 5 and 6 is the ignitor retraction completed 0.058 second after beginning of retraction.

Frame 1 in figure 17(b), showing selected schlieren frames of run 3, is the frame just prior to ignition. The ignitor is seen extending from the lower right to a point near the model surface just upstream of the model base. Combustion is first seen in frame 2 as compared with frame 1 of figure 17(a). In figure 17(b), frame 2 is quite close to the instant of ignition as shown by the small region of combustion ahead of the ignitor.

Subsequent frames 3 to 10 show the upstream advance of the flame to the fuel orifices and enlargement of the combustion region. The combustion and associated flow shown in frames 9 and 10 are characteristic of the steady-state combustion of run 3, and frames 9 and 10 are similar to those taken later during combustion.

4139

CJ-3

APPENDIX D

CALCULATION OF AXIAL FORCES

The axial (drag and thrust) forces acting on a body of revolution at zero incidence to a supersonic stream may be divided into the axial components of two types of forces, namely, friction forces and pressure forces acting normal to the body surface. The axial components of the pressure forces may be considered as being subdivided into axial forces acting on the forebody (having no rearward-facing surfaces) and those acting on the afterbody (having no forward-facing surfaces). Thus, the axial components of the pressure forces acting on the forebody are drag components, and the components acting on the afterbody and base are thrust components. The body of revolution used in this investigation has a near-parabolic forebody, a cylindrical afterbody without boattailing, and a blunt base. Therefore, at zero incidence (in a supersonic airstream), the axial forces acting on this model are the force on the model base, the sum of the axial components of the normal pressures acting on the forebody, and the skin friction on both the forebody and afterbody. In the usual nonburning aerodynamics, the normal-pressure contributions to the axial forces on this model are given in terms of a wave drag and a base drag, quantities obtained relative to the free-stream static pressures. However, in the following discussion it will be more convenient to consider the forces calculated from the absolute pressures on the model.

Since the measurements made included only model surface pressures and did not include force balance values, no information on the skin-friction portion of the drag was obtained. Skin-friction drag without combustion was calculated from the measured skin-friction drag coefficient given in reference 13 for the identical body of revolution at comparable Reynolds number and a Mach number of 3.12. For a Reynolds number of 8.0×10^6, two values for skin-friction drag coefficients (based on frontal area) may be obtained from figure 19 of reference 13. The value obtained from boundary-layer calculation is about 0.054, and that value obtained from force and pressure measurements is 0.072. If the greater (more conservative) value is used, then for a free-stream static pressure of 2.93 inches of mercury and Mach number of 2.47, the skin-friction drag without combustion is 1.07 pounds.

The skin-friction drag of the model during combustion is estimated by assuming that the combustion results in increasing the skin-friction by a factor of 2 or less. For the body surface adjacent to the combustion, a factor increase of 2 in the skin friction would require a similar factor increase in the product of dynamic viscosity and velocity gradient at the wall. If the Mach number is subsonic or supersonic, the order of

magnitude calculations on the viscosity and velocity in the combustion region still indicate that the values of local skin friction during combustion are actually not greater than this factor of 2, but are probably less than twice the values without combustion. This calculation does not consider the possible additional friction which would result from ash deposits on the surface during the burning. The skin-friction drag during combustion is calculated by assuming that the increased skin-friction drag coefficient of 0.144 acts only on the wetted surface area adjacent to the burning. This surface area consists of the cylindrical afterbody of the model. Calculated on this basis, the skin-friction drag during combustion is 1.69 pounds. Therefore, during combustion (using the average of good combustion data) the axial forces acting on the body of revolution are

Model skin friction, lb	-1.69
Axial force on forebody, lb	-3.92
Force on base, lb	5.88
Sum of axial forces, lb	0.27

where the plus and minus signs indicate axial forces acting in the upstream and downstream direction, respectively.

The axial forces without combustion are as follows:

Model skin friction, lb	-1.07
Axial force on forebody, lb	-3.92
Force on base, lb	1.61
Sum of axial forces, lb	-3.38

The reduction in total drag is also appreciable for the weak combustion runs. For example, for run 10 with burning only downstream of the model base, the axial forces acting on the body of revolution are

Model skin friction, lb	-1.07
Axial force on forebody, lb	-3.92
Force on base, lb	4.69
Sum of axial forces, lb	-0.30

Since the fuel burned only downstream of the model base, the skin-friction drag is calculated for the case where there is no combustion adjacent to the surface area.

4139

4139

REFERENCES

1. Hicks, Bruce L., Montgomery, Donald J., and Wasserman, Robert H.: On the One-Dimensional Theory of Steady Compressible Fluid Flow in Ducts with Friction and Heat Addition. Jour. Appl. Phys., vol. 18, no. 10, Oct. 1947, pp. 891-903.

2. Shapiro, Ascher H., and Hawthorne, W. R.: The Mechanics and Thermodynamics of Steady One-Dimensional Gas Flow. Jour. Appl. Mech., vol. 14, no. 4, Dec. 1947, pp. A317-A336.

3. Pinkel, I. Irving, and Serafini, John S.: Graphical Method for Obtaining Flow Field in Two-Dimensional Supersonic Stream to Which Heat Is Added. NACA TN 2206, 1950.

4. Pinkel, I. Irving, Serafini, John S., and Gregg, John L.: Pressure Distribution and Aerodynamic Coefficients Associated with Heat Addition to Supersonic Air Stream Adjacent to Two-Dimensional Supersonic Wing. NACA RM E51K26, 1952.

5. Smith, E. H., and Davis T.: The Creation of Thrust and Lift by Combustion on External Surfaces of Airfoils. Smith and Davis, Physicists, Silver Spring (Md.), Sept. 1, 1952. (Bur. Ord., Dept. Navy Contract NOrd 12141.)

6. Fletcher, Edward A., Dorsch, Robert G., and Gerstein, Melvin: Combustion of Aluminum Borohydride in a Supersonic Wind Tunnel. NACA RM E55D07a, 1955.

7. Dorsch, Robert G., Serafini, John S., and Fletcher, Edward A.: A Preliminary Investigation of Static-Pressure Changes Associated with Combustion of Aluminum Borohydride in a Supersonic Wind Tunnel. NACA RM E55F07, 1955.

8. Dorsch, Robert G., Serafini, John S., and Fletcher, Edward A.: Exploratory Investigation of the Aerodynamic Effects of External Combustion of Aluminum Borohydride in Airstream Adjacent to Flat Plate in Mach 2.46 Tunnel. NACA RM E57E16, 1957.

9. Cortright, Edgar M., Jr., and Schroeder, Albert H.: Preliminary Investigation of Effectiveness of Base Bleed in Reducing Drag of Blunt-Base Bodies in Supersonic Stream. NACA RM E51A26, 1951.

10. Cortright, Edgar M., Jr., and Schroeder, Albert H.: Investigation at Mach Number 1.91 of Side and Base Pressure Distributions over Conical Boattails Without and With Jet Flow Issuing from Base. NACA RM E51F26, 1951.

11. Scanland, T. S., and Hebrank, W. H.: Drag Reduction Through Heat Addition to the Wake of Supersonic Missiles. Memo. Rep. 596, Ballistic Res. Labs., Aberdeen Proving Ground (Md.), June 1952. (Proj. No. TB3-0110, Res. and Dev. Div., Ord. Corps.)

12. Baker, W. T., Davis, T., and Matthews, S. E.: Reduction of Drag of a Projectile in a Supersonic Stream by the Combustion of Hydrogen in the Turbulent Wake. CM-763, Appl. Phys. Lab., The John Hopkins Univ., June 4, 1951. (Contract NOrd 7386, with Bur. Ord., U.S. Navy.)

13. Jack, John R., and Burgess, Warren C.: Aerodynamics of Slender Bodies at Mach Number of 3.12 and Reynolds numbers from 2×10^6 to 15×10^6. I - Body of Revolution with Near-Parabolic Forebody and Cylindrical Afterbody. NACA RM E51H13, 1951.

14. Chapman, Dean R.: An Analysis of Base Pressure at Supersonic Velocities and Comparison with Experiment. NACA Rep. 1051, 1951. (Supersedes NACA TN 2137.)

15. Reller, John O., Jr., and Hamaker, Frank M.: An Experimental Investigation of the Base Pressure Characteristics of Nonlifting Bodies of Revolution at Mach Numbers from 2.73 to 4.98. NACA TN 3393, 1955. (Supersedes NACA RM A52E20.)

16. Love, Eugene S., and O'Donnel, Robert M.: Investigations at Supersonic Speeds of the Base Pressure on Bodies of Revolution With and Without Sweptback Stabilizing Fins. NACA RM L52J21a, 1952.

4139

4139

TABLE I. - LOCATIONS OF SURFACE STATIC-PRESSURE, BASE-PRESSURE, AND FUEL ORIFICES

[Orifices numbered]

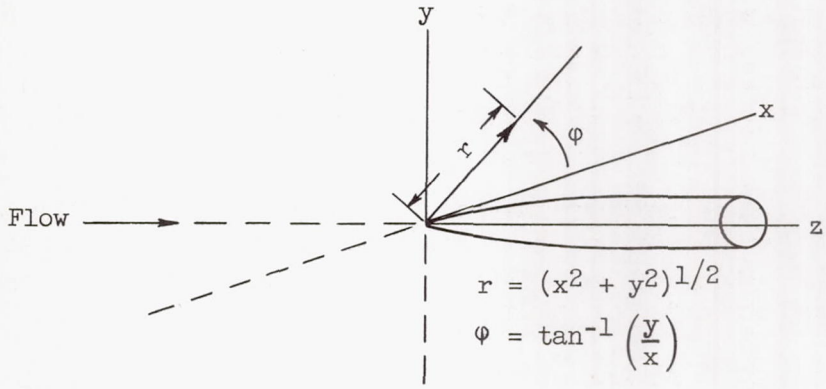

(a) Surface static-pressure orifices

Axial distance, z, in.	Meridian angle, φ, deg	Axial distance, z, in.	Meridian angle, φ, deg			
	90		90	45	0	-90
2	1	13	9			
4	2	14	10			
6	3	15	11			
8	4	16	12			
9	5	17.5	13	17	18	19
10	6	18.75	14			
11	7	20	15			
12	8	20.5	16	20	21	

(b) Base-pressure orifices

Radial distance, r, in.	Meridian angle, φ, deg				
	90	60	30	0	-90
0.48	30				
.63	26	27	28	29	31
.81	22	23	24	25	

(c) Fuel orifices

Axial distance, z, in.	Radial distance, r, in.	Meridian angle, φ, deg			
10.5	0.875	-90	0	90	180

TABLE II. - SURFACE AND BASE STATIC-PRESSURE CHANGES RESULTING FROM COMBUSTION ABOUT BODY OF REVOLUTION IN 2.47 MACH AIRSTREAM

(a) Pressure changes for surface static-pressure taps

Run	Stagnation temperature, °F	Stagnation pressure, in. Hg	Helium injector pressure, lb/sq in. gage	Injector fuel charge, cc	Pressure-change pulse length +0.2, sec	Fuel injection rate, w_f, cc/sec	Pressure changes of numbered model statics, in. Hg																			
							2	3	4	5	6	7	8	9	10	11	12	13	14	15	16	17	18	19	20	21
[a]1	101	47.54	100	26	3.80	6.8					0	0.71	1.09	0.79	0.33	0.13	0	-0.11				-0.12	-0.10	-0.07		
2	103	47.25	100	26	2.22	[b]11.7					0	2.11	(e)	2.03	1.97	1.97	2.03	2.03				2.02	2.03	2.05		
3	97	47.84	50	25	2.18	[b]11.5	0	0.02	0.02	0.02	0		2.38		1.86	2.02	2.01		1.96	2.04	1.93		1.93		1.92	1.96
[a]4	100	47.96	50	25	2.36	[b]10.6	0	0	0	0	.06		2.36		1.55	1.70	1.80		1.79	1.87	1.82		1.71		1.77	1.80
5	99	47.63	50	28	2.56	[b]10.9	0	.01	.01	.01	.09		2.19		1.85	2.02	1.97		1.93	2.03	1.97		1.88		1.94	1.96
6	98	47.66	50	25	3.51	7.1	0	0	0	.02	.08		1.42		1.57	1.60	1.58		1.54	1.65	1.62		1.60		1.62	1.61
7	97	47.20	50	25	2.27	[b]11.0	0	0	0	.02	.03	2.27	2.56	2.01	1.85		2.04	2.06	2.02			2.02	1.88	2.07	2.02	
[a]8	99	47.37	50	25	4.16	[c]6.0	0	0	0	0	0	(d)	(d)	(d)	(d)		(d)	(d)	0			(d)	0	(d)		
9	100	48.03	50	28	2.32	[b]12.1	0			0	.04	2.72	2.46	1.95	(e)	2.03	2.16	2.39	2.21		2.25	2.19		2.23	2.14	2.15
[a]10	100	47.82	50	25	3.12	[c]8.0	0			0	0	0	0	0	0	0	0	0	0		0	0		0	0	0
11	100	47.94	50	25	2.37	[b]10.6	0			0	0	2.18	1.88	1.91	2.02	2.12	2.07	2.12	2.08		2.07	2.08		2.07	2.01	2.10
[a]12	98	48.12	50	25	1.96	[b]12.8	0			0	.01	1.95	2.56	(e)	1.45	1.61	1.90	2.18	2.04		2.06	2.00		1.97	2.00	2.05

[a]Ignitor did not retract.

[b]Good combustion run.

[c]Combustion only downstream of base.

[d]No readable steady-state pulses (large initial pulse occurs and drops off to zero).

[e]Plugged pressure-change pulse.

4139

TABLE II. - Concluded. SURFACE AND BASE STATIC-PRESSURE CHANGES RESULTING FROM COMBUSTION ABOUT BODY OF REVOLUTION IN 2.47 MACH AIRSTREAM

(b) Pressure-changes for base static-pressure taps (corrected for ignitor retraction where applicable)

Run	Pressure changes of numbered model statics, in. Hg									
	22	23	24	25	26	27	28	29	30	31
[a]1	1.70	1.82	1.80	1.82	1.68	1.70	1.86	1.70	1.65	1.65
2	3.54	3.63	3.56	3.61	3.63	3.56	3.47	3.47	3.58	3.57
3		3.65		3.68	3.61		3.54			
[a]4		3.68		3.78	3.65		3.62			
5		3.60		3.53	3.61		3.58			
6		3.22		3.26	3.17		3.16			
7	3.69	3.72	3.66	3.69	3.70	3.63	3.64	3.67	3.75	3.60
[a]8	1.40	1.51	1.45	1.49	1.42	1.45	1.46	1.45	1.40	1.30
9	3.90	3.78	3.82	3.83	3.68	(b)	3.69	3.70	3.85	3.78
[a]10	2.68	2.80	2.94	2.85	2.52	2.75	2.80	2.84	2.64	2.78
11	3.74		3.78			3.57		3.68	3.71	
[a]12	3.73		3.78			3.80		3.52	3.72	

[a]Ignitor did not retract.

[b]Plugged pressure-change pulse.

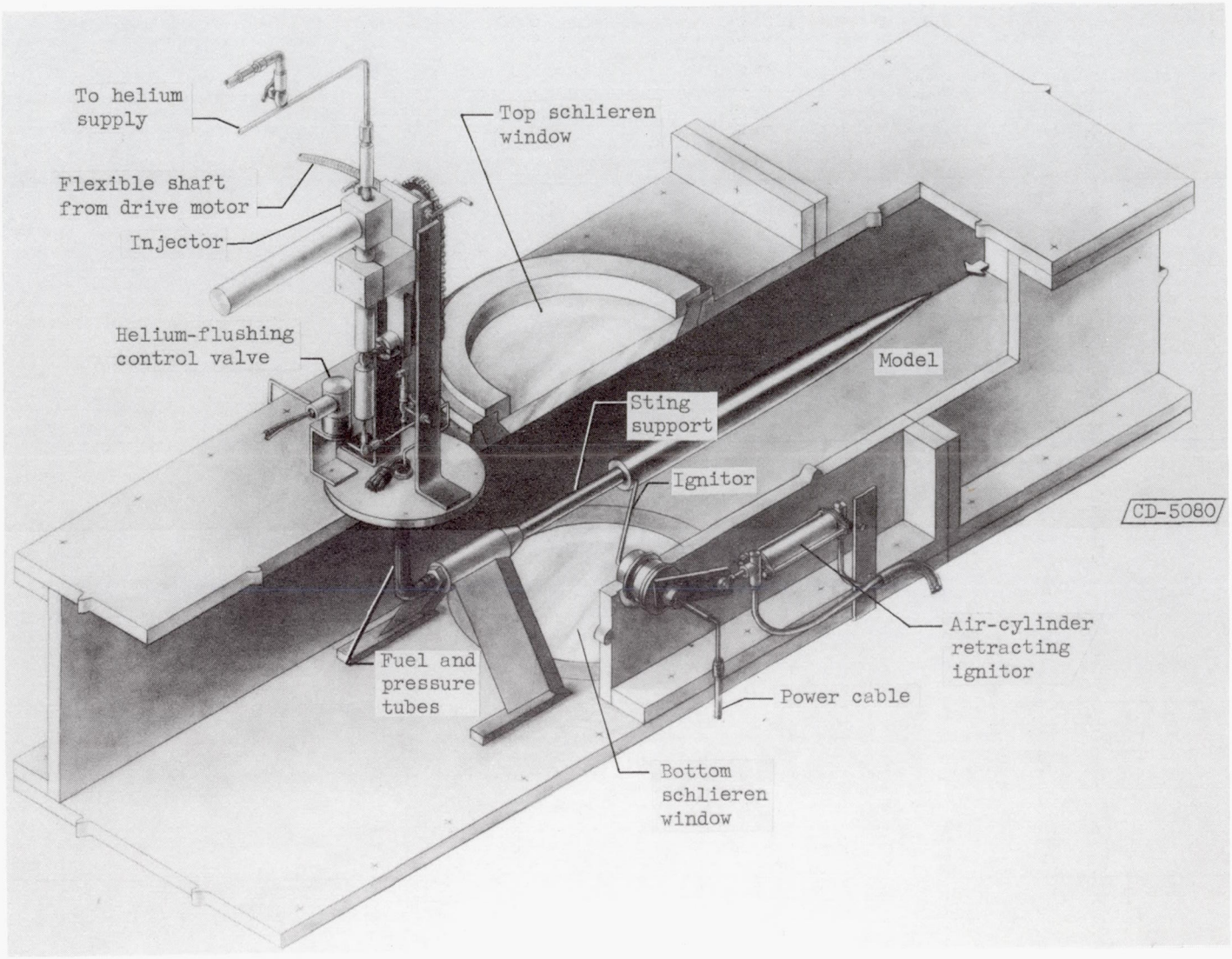

Figure 1. - Sketch of wind-tunnel, model, fuel-injector, and ignitor system.

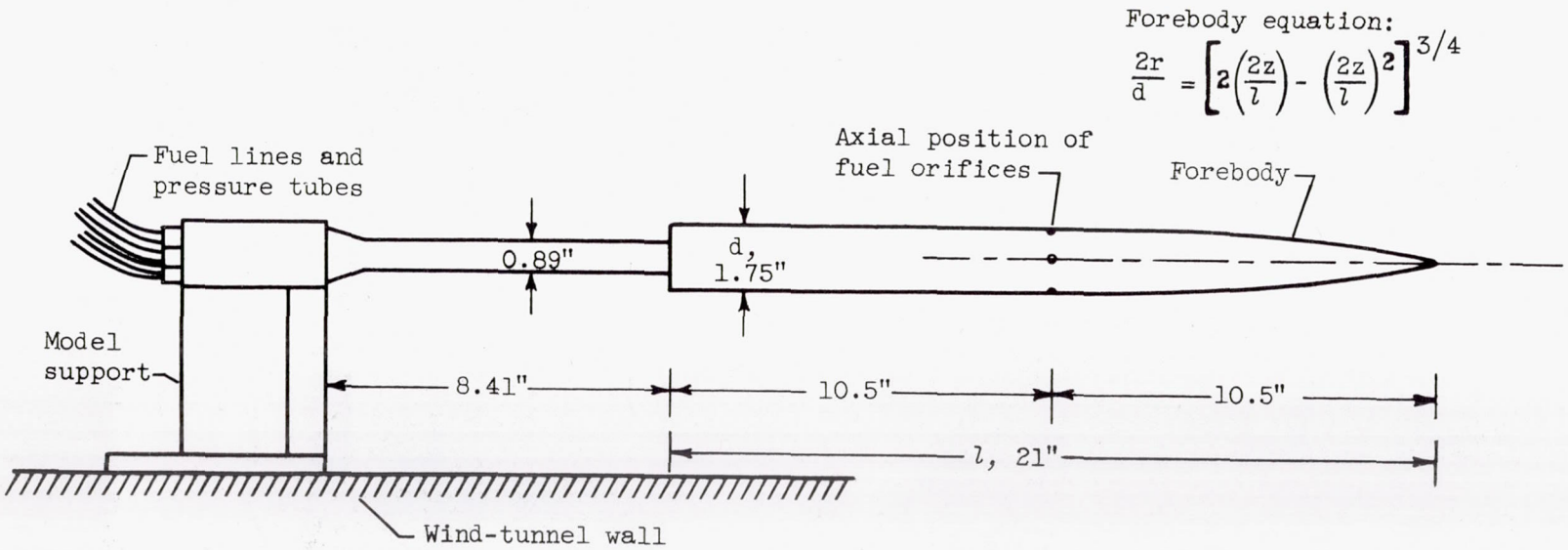

Figure 2. - Sketch of model and sting support.

4139

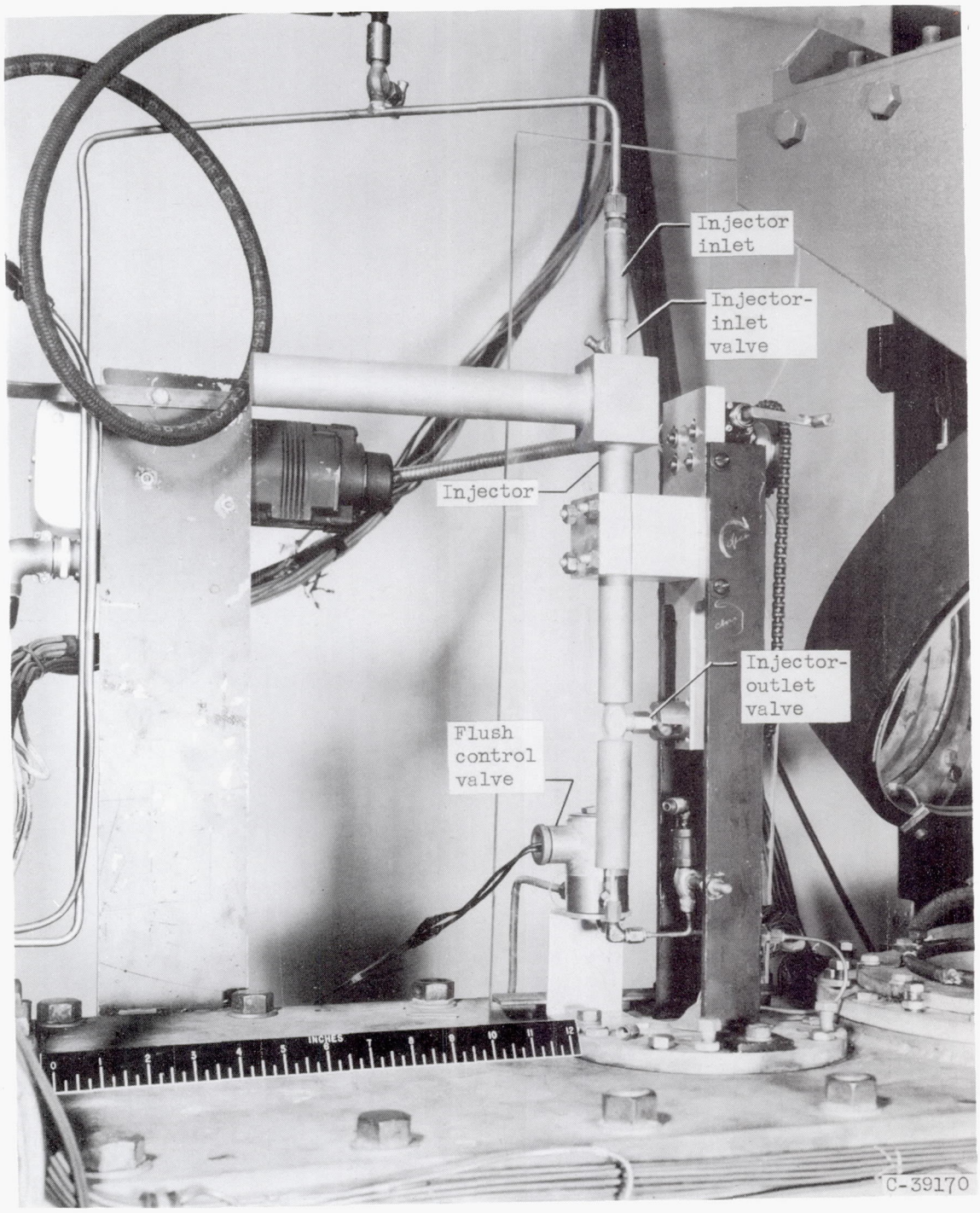

Figure 3. - Fuel-injector installation.

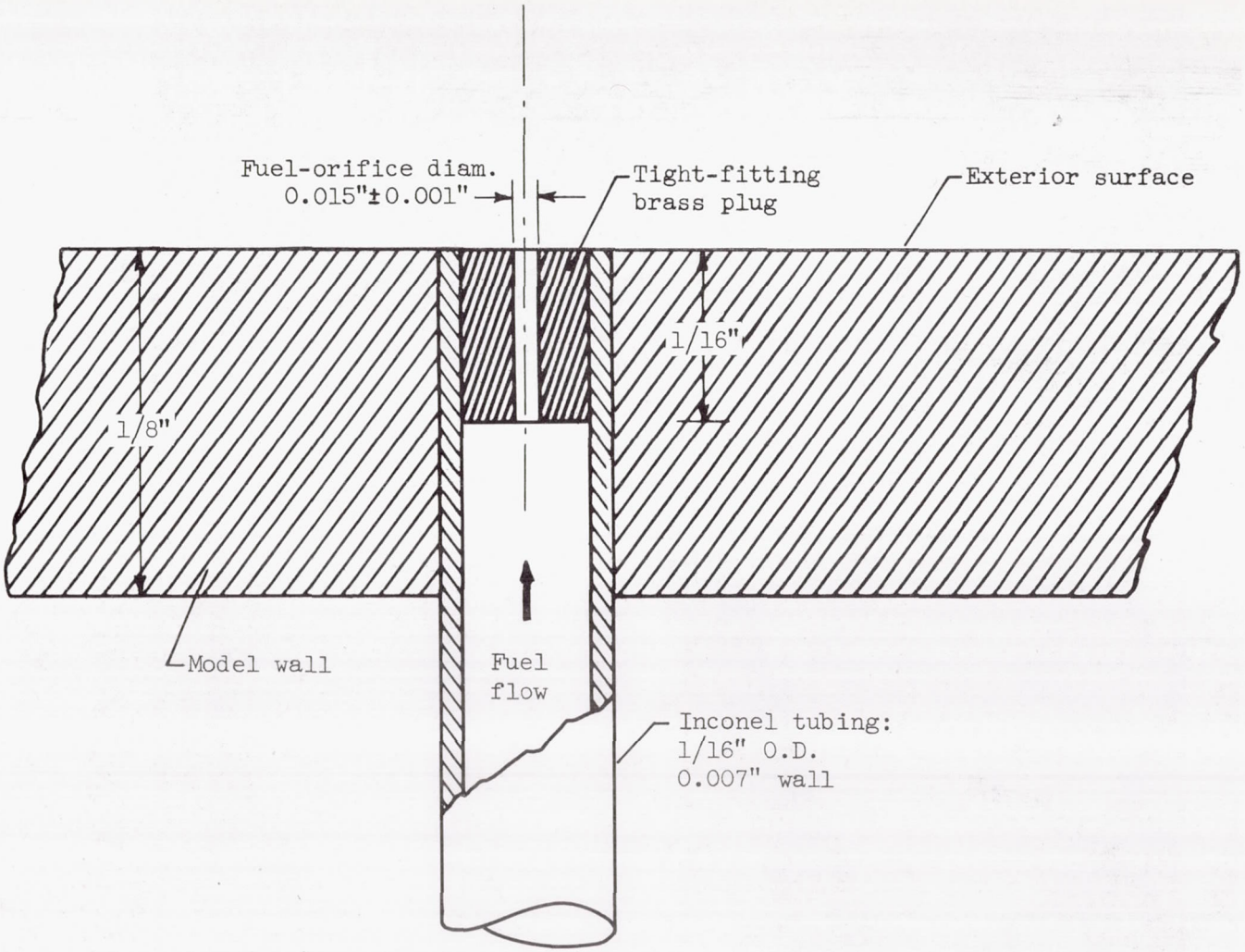

Figure 4. - Details of fuel-orifice construction.

4139

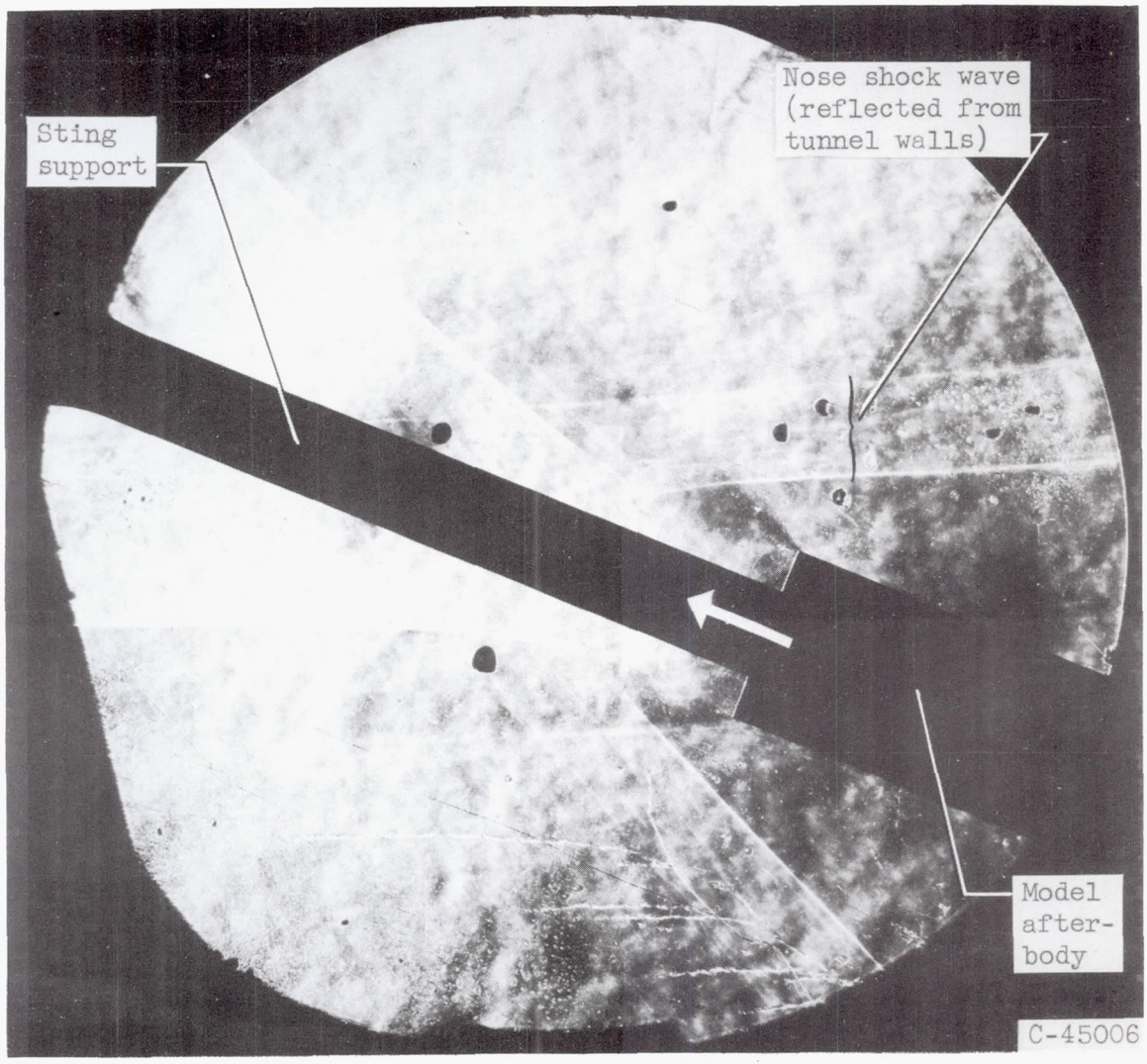

Figure 5. - Schlieren photograph of flow about model (ignitor extended).

4139

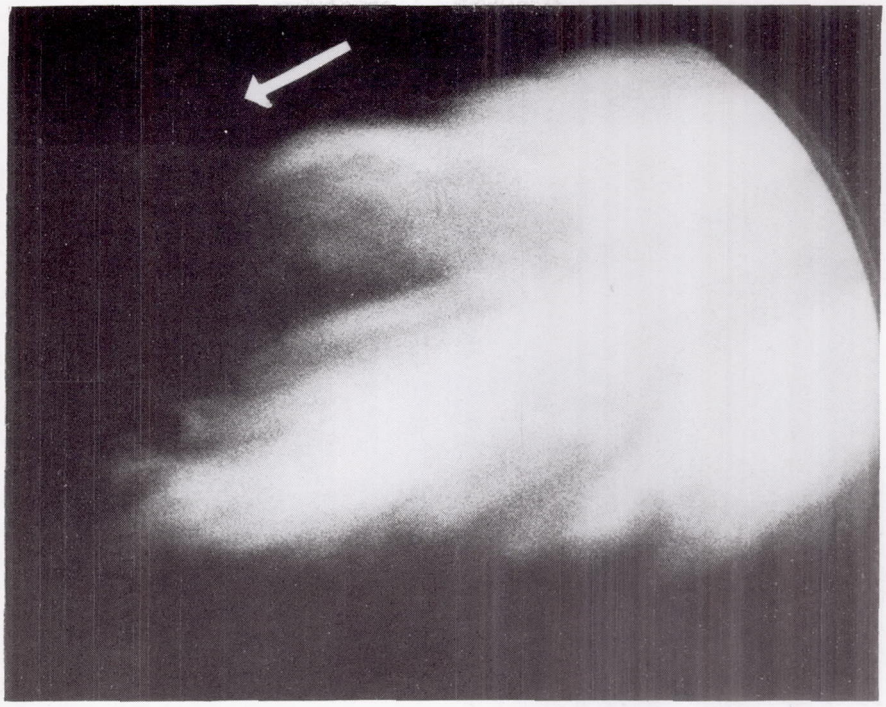

Frame 1

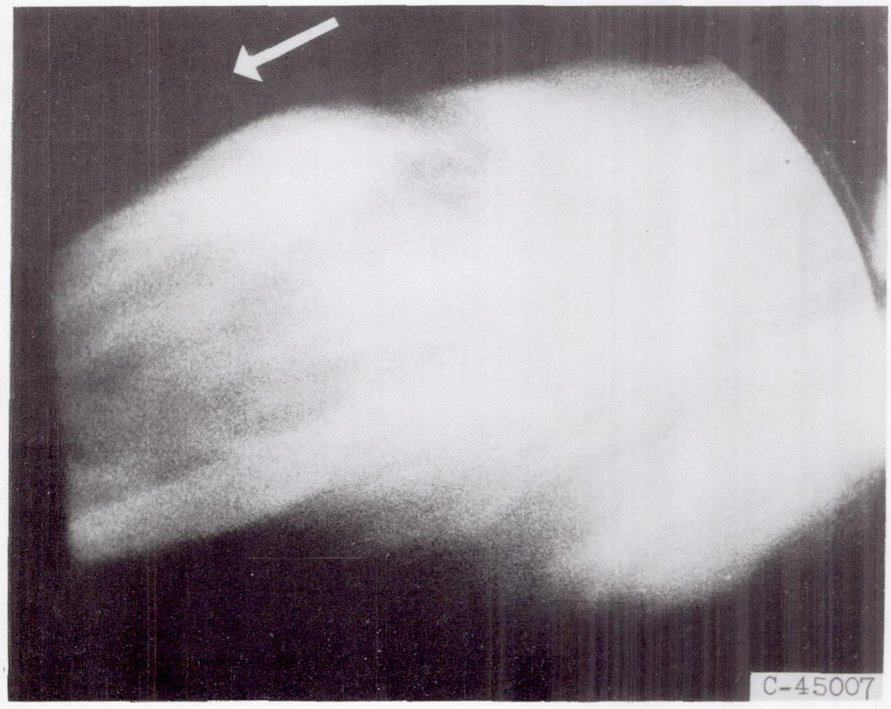

Frame 2

Figure 6. - Directly photographed motion-picture frames showing typical steady-state combustion (run 9). Camera speed, 4200 frames per second.

4139

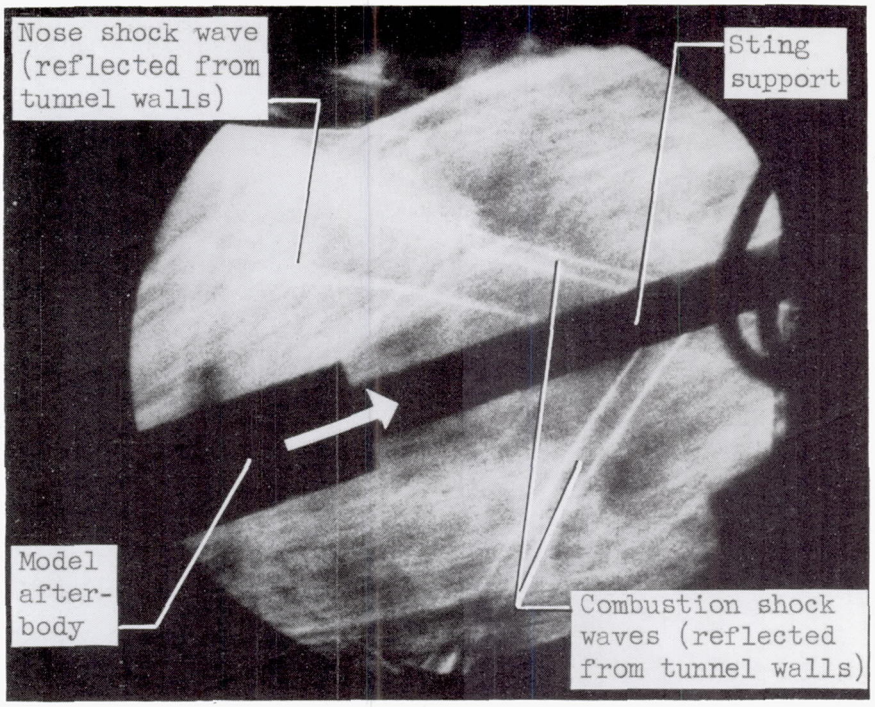

Frame 1

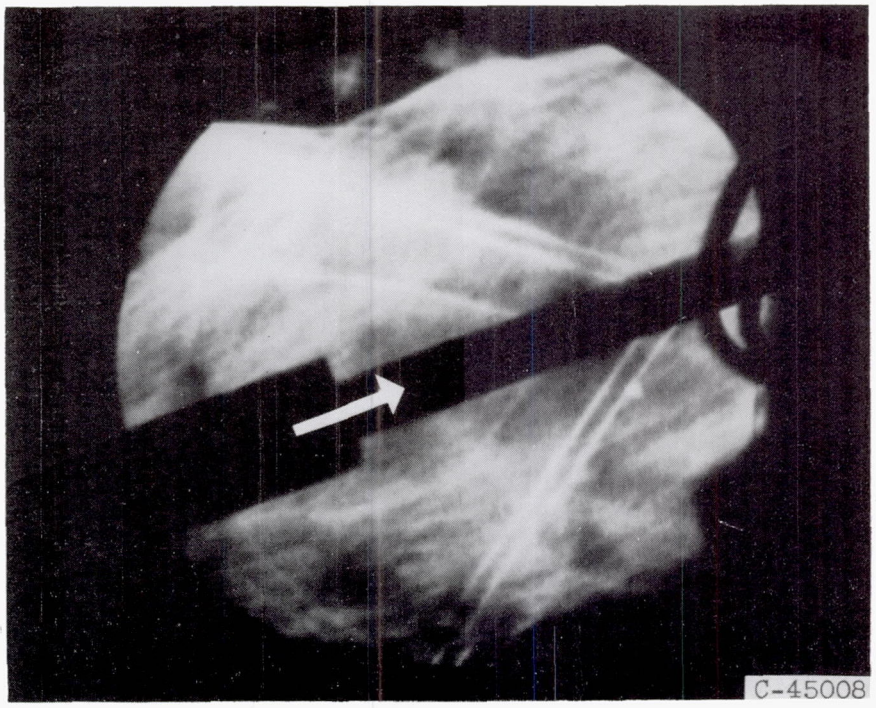

Frame 2

Figure 7. - Schlieren motion-picture frames showing typical steady-state combustion (run 9). Camera speed, 4500 frames per second.

4139

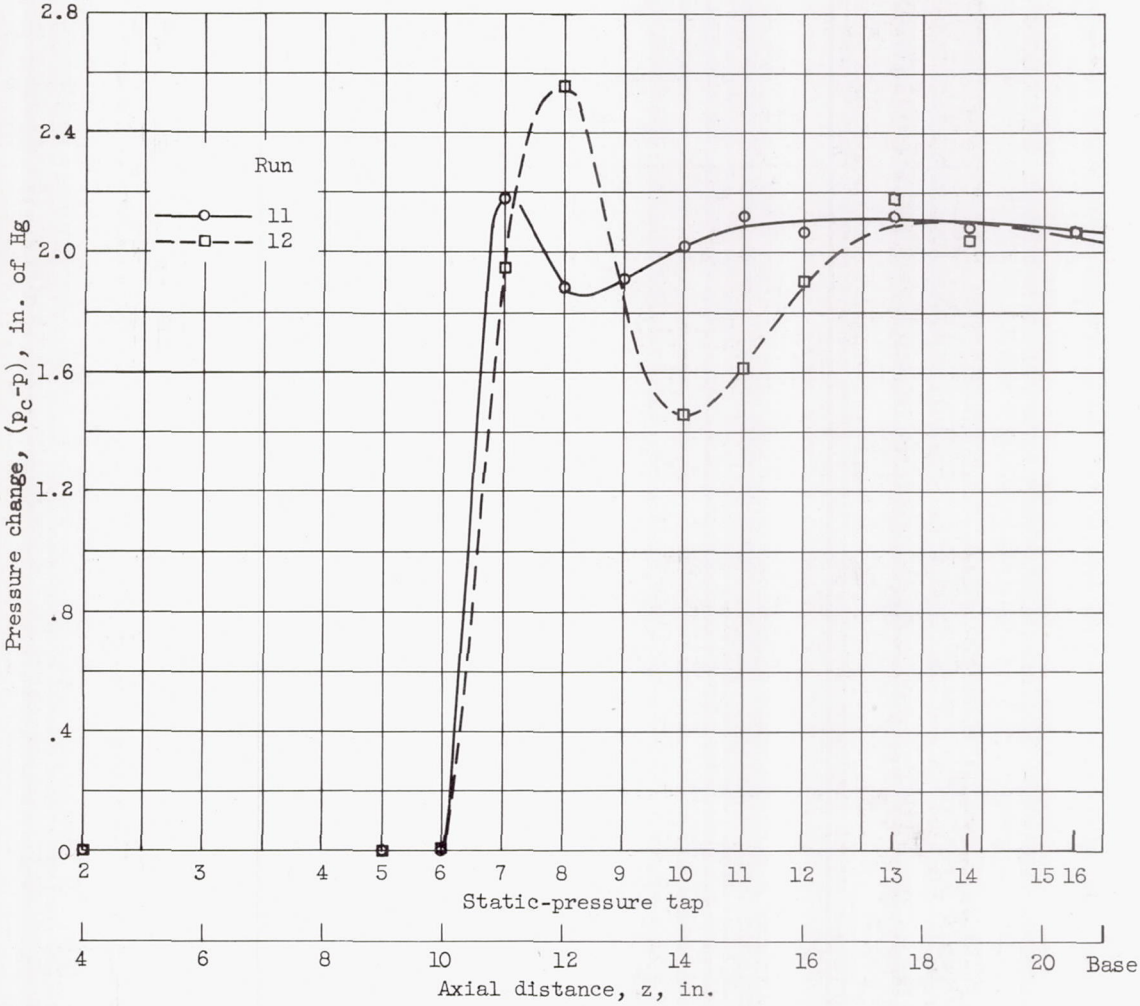

(a) Typical variations due to good combustion.

Figure 8. - Axial static-pressure increases. Meridian angle, 90°.

4139

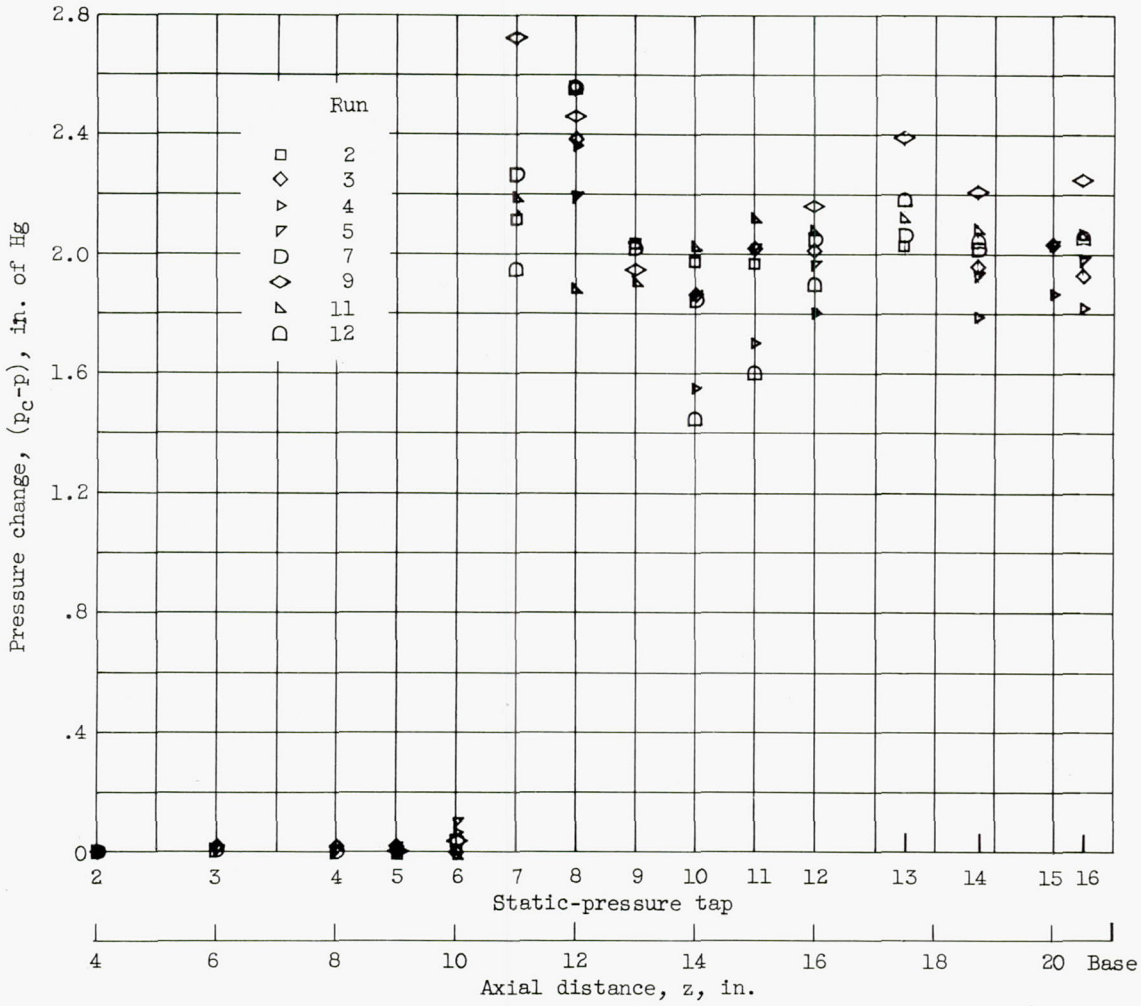

(b) Increases due to all good combustion runs (2, 3, 4, 5, 7, 9, 11, and 12).

Figure 8. - Concluded. Axial static-pressure increases. Meridian angle, 90°.

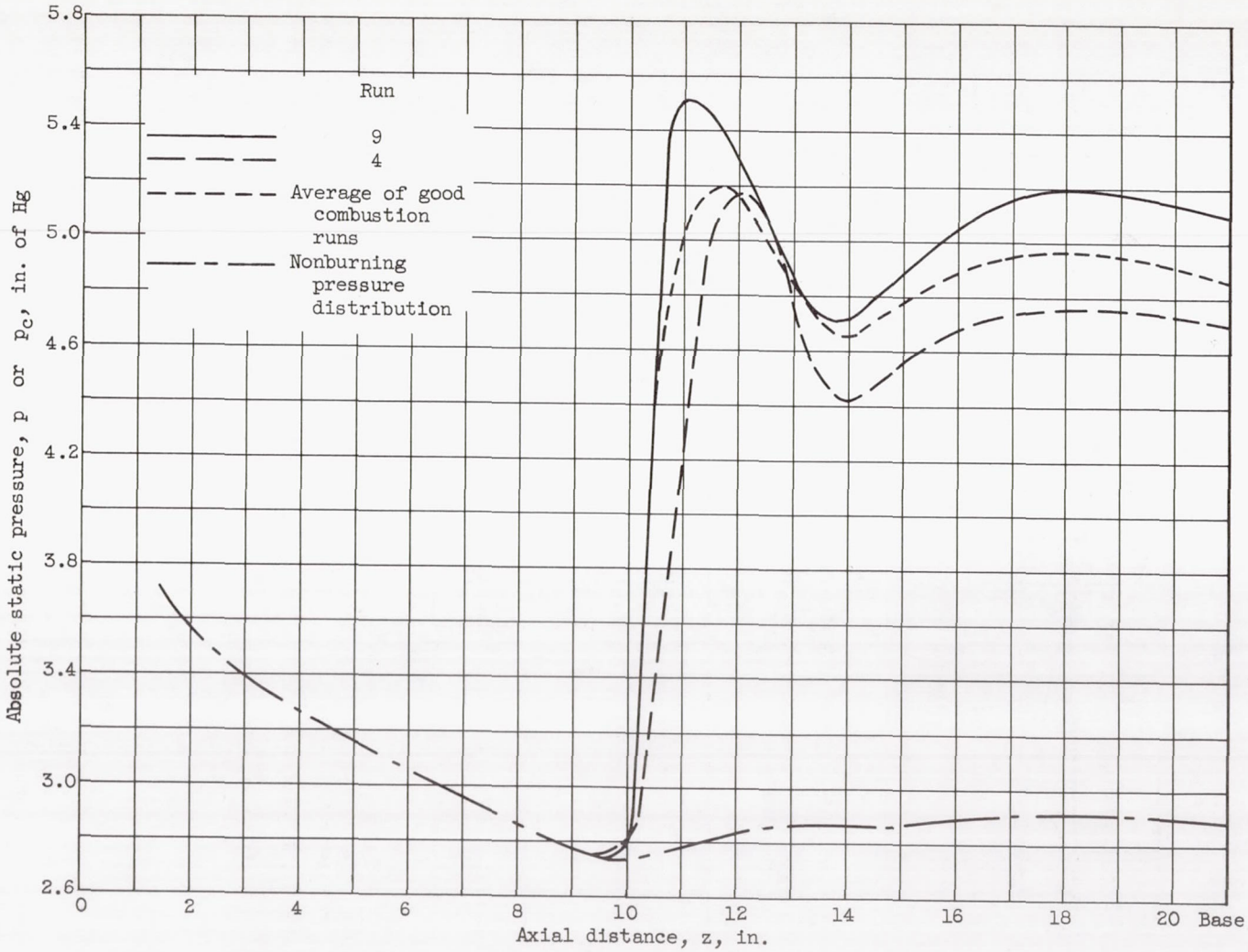

Figure 9. - Average, maximum, and minimum axial variations of the absolute pressures resulting from good combustion runs, and comparison with the absolute pressures occurring without combustion. Total pressure, 47.75 inches of mercury.

4139

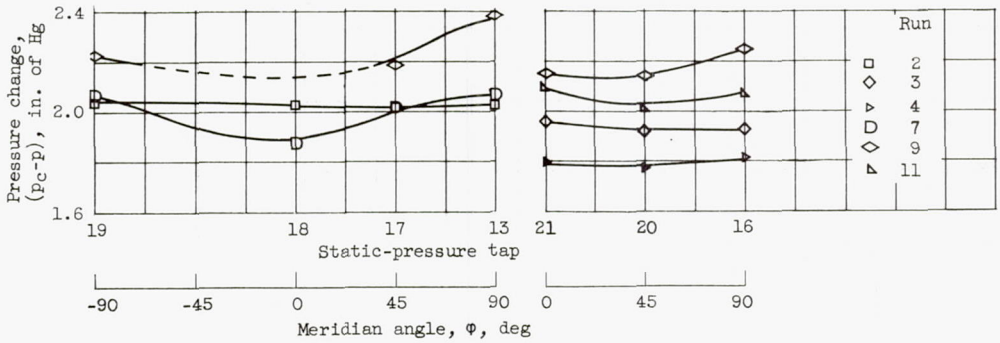

(a) Axial distance, 17.5 inches. (b) Axial distance, 20.5 inches.

Figure 10. - Typical meridional variations of pressure changes resulting from good combustion runs.

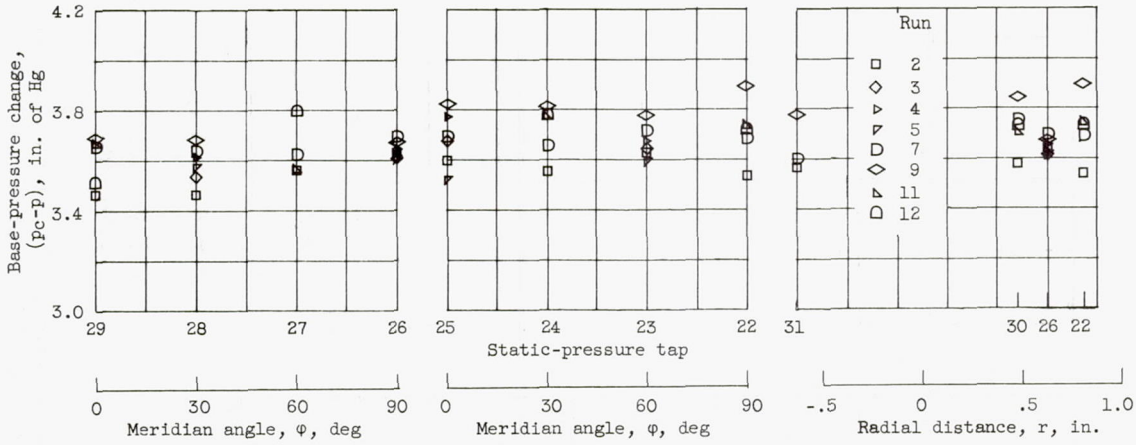

(a) Radial distance, 0.63 inch. (b) Radial distance, 0.81 inch. (c) Meridian angle, 90°.

Figure 11. - Base-pressure increases resulting from good combustion runs. Axial distance, 21 inches.

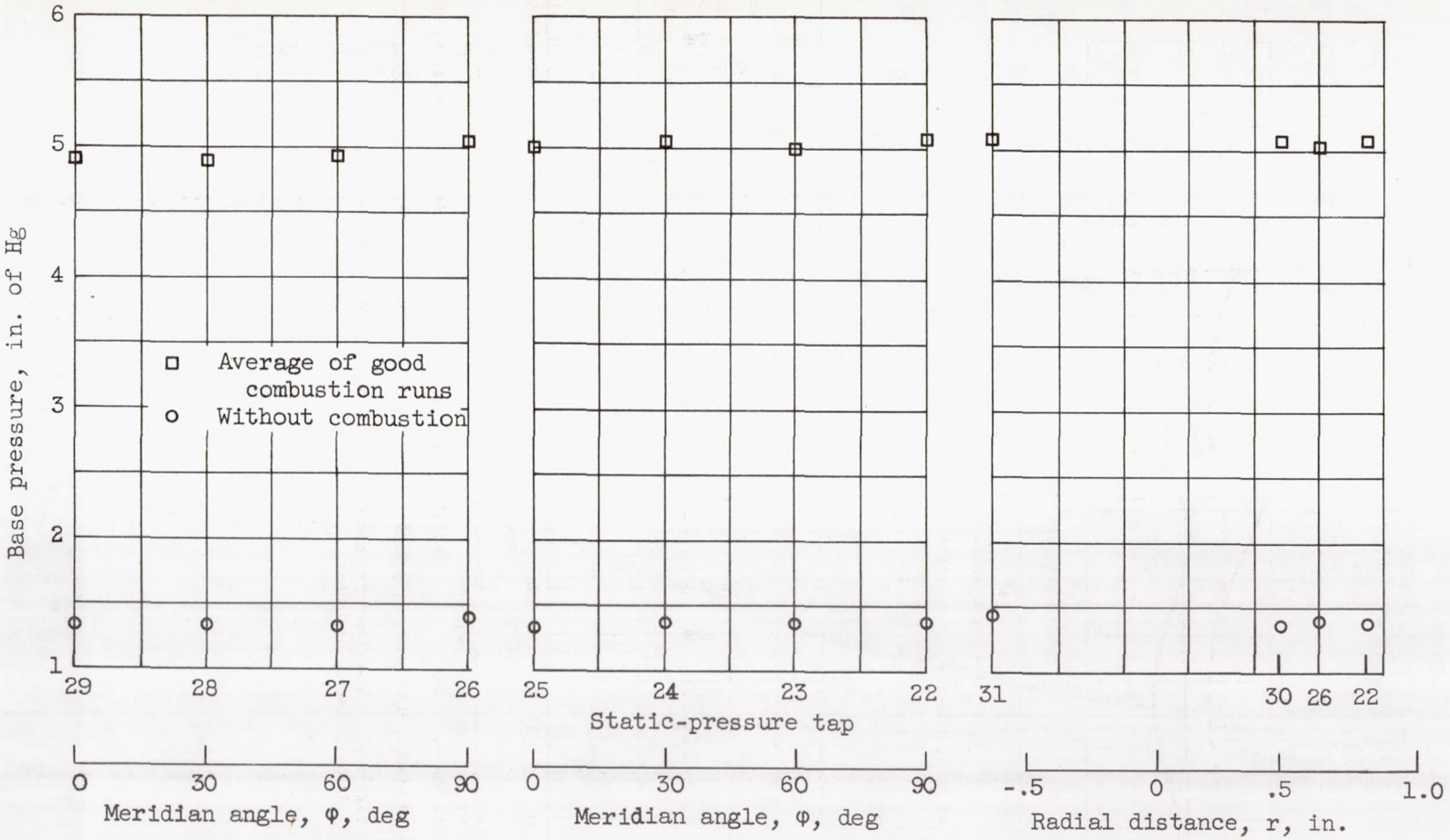

(a) Radial distance, 0.63 inch.

(b) Radial distance, 0.81 inch.

(c) Meridian angle, 90°.

Figure 12. - Comparison of base-pressures with and without combustion in terms of absolute pressures. Axial distance, 21 inches.

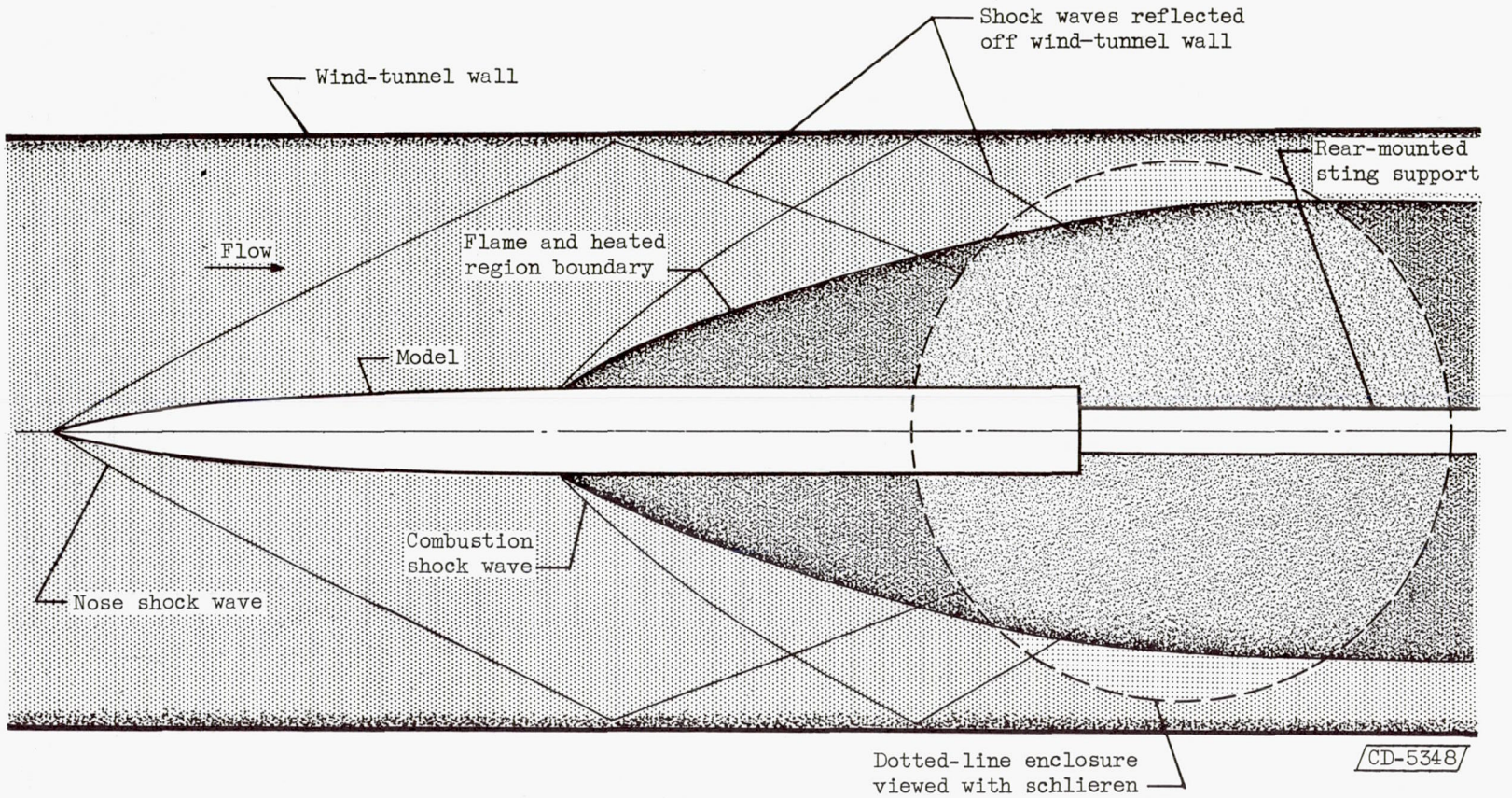

Figure 13. - Combustion and associated flow about the model for the horizontal plane through the model centerline (run 9).

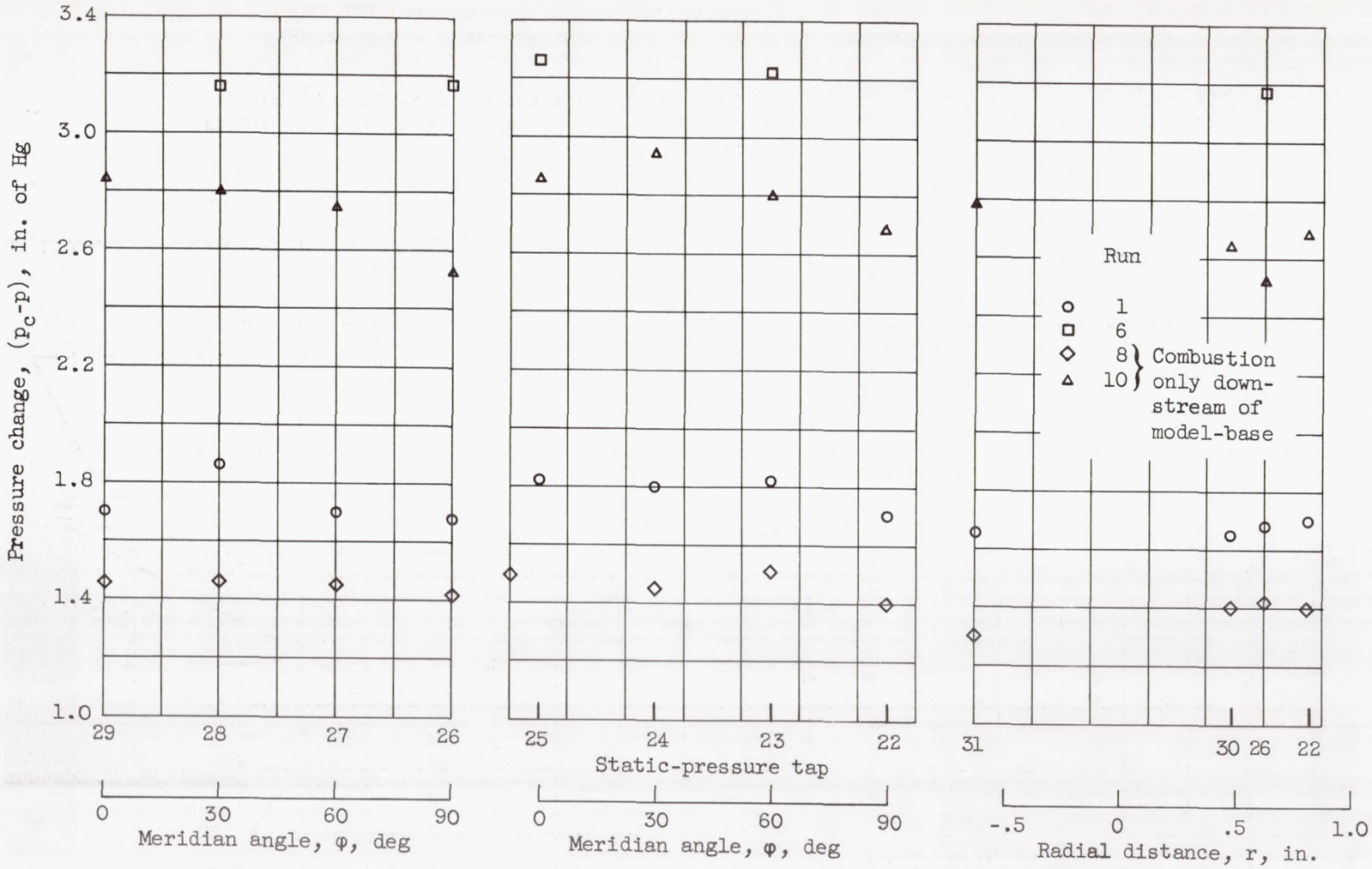

(a) Radial distance, 0.63 inch. (b) Radial distance, 0.81 inch. (c) Meridian angle, 90°.

Figure 14. - Pressure changes resulting from weak combustion runs. Axial distance, 21 inches.

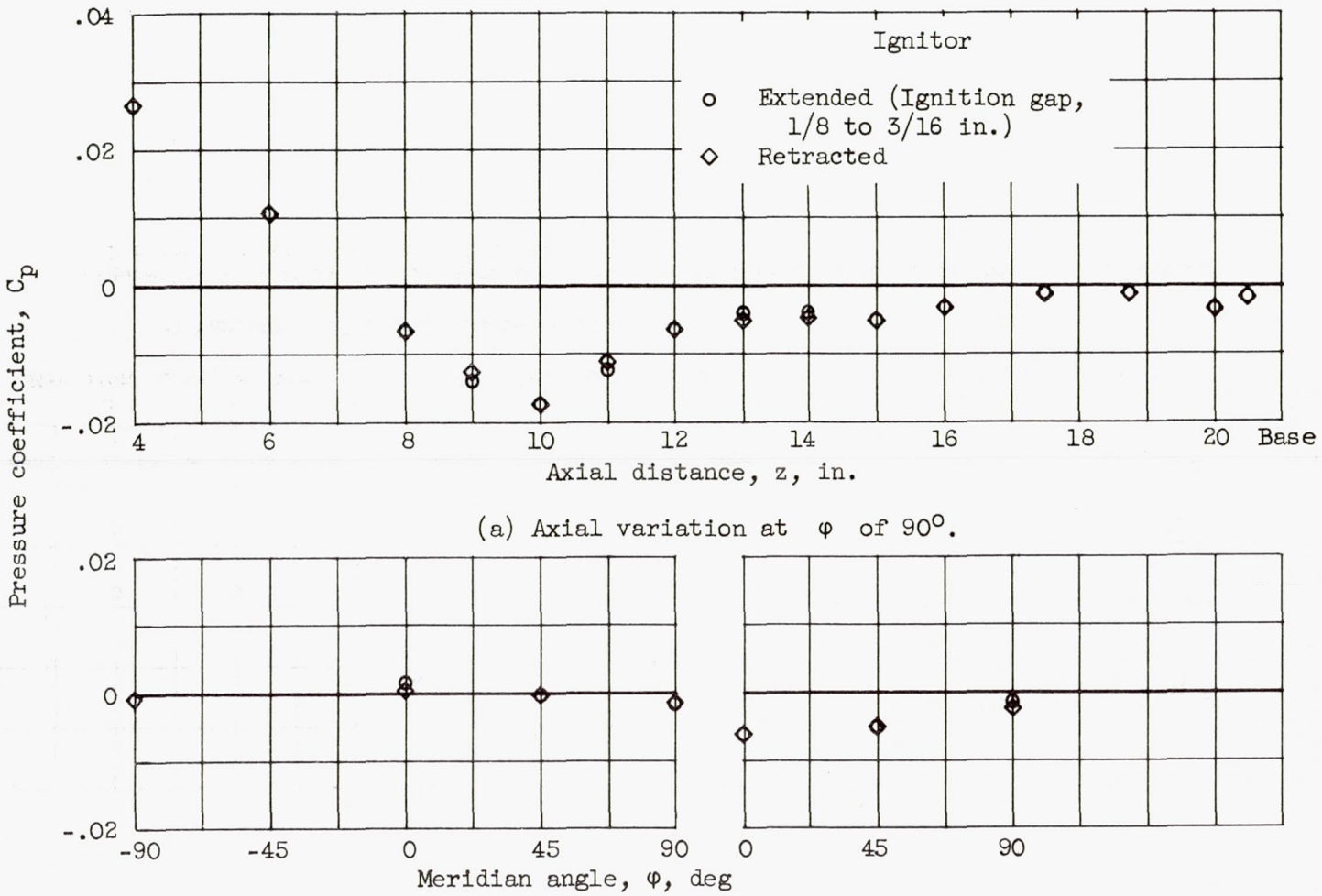

(a) Axial variation at φ of 90°.

(b) Meridional variation at the axial distances of 17.5 and 20.5 inches.

Figure 15. - Pressure-coefficient distribution about model without combustion for ignitor retracted and extended.

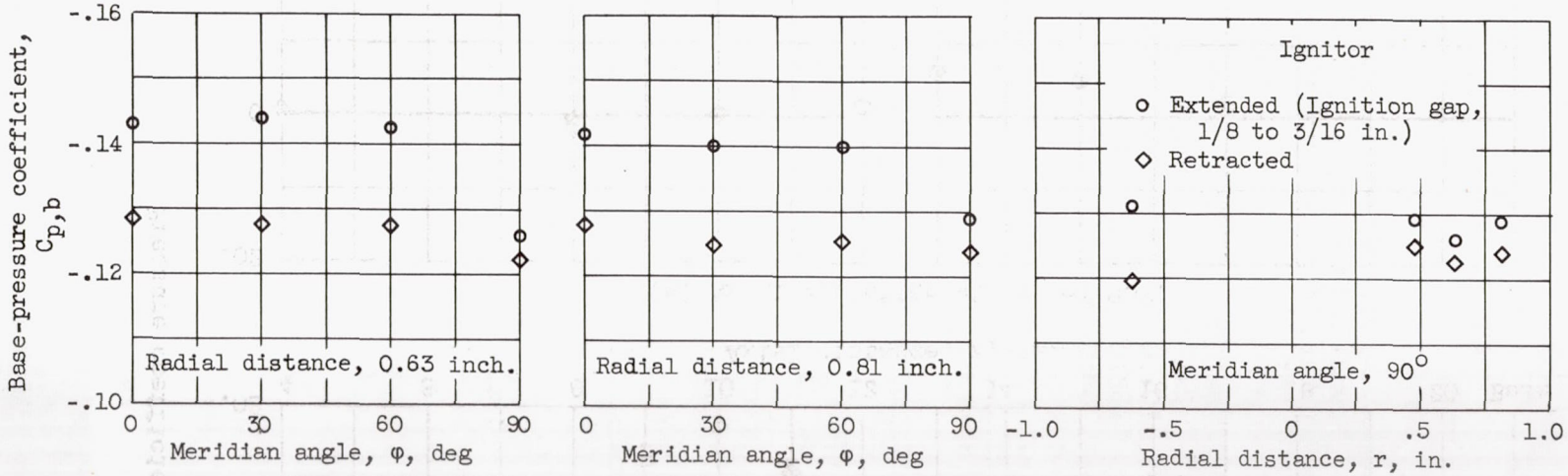

(c) Variation of base-pressure coefficient. Axial distance, 21 inches.

Figure 15. - Concluded. Pressure-coefficient distribution about model without combustion for ignitor retracted and extended.

4139

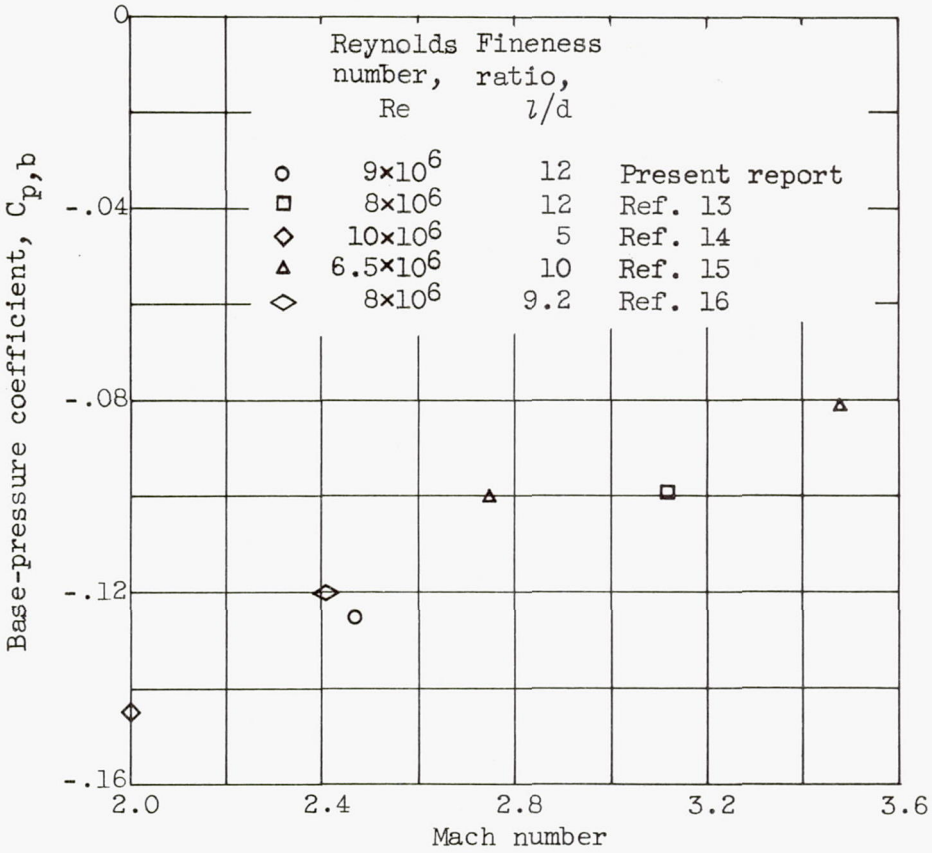

Figure 16. - Comparison with other reported results of average base-pressure coefficient obtained without combustion.

4139

CJ-6

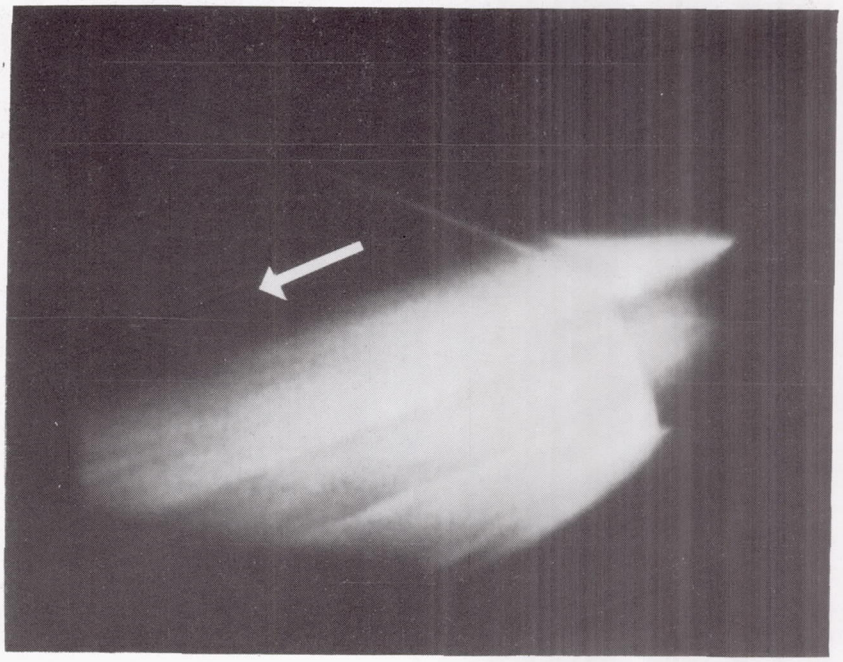

Frame 1 (time interval, 0 sec; camera speed, 1310 frames/sec.)

Frame 2 (time interval, 0.001 sec; camera speed, 1310 frames/sec.)

(a) Directly-photographed motion-picture frames.

Figure 17. - Single motion-picture frames of run 3 showing the development from ignition of a typical good combustion run.

4139

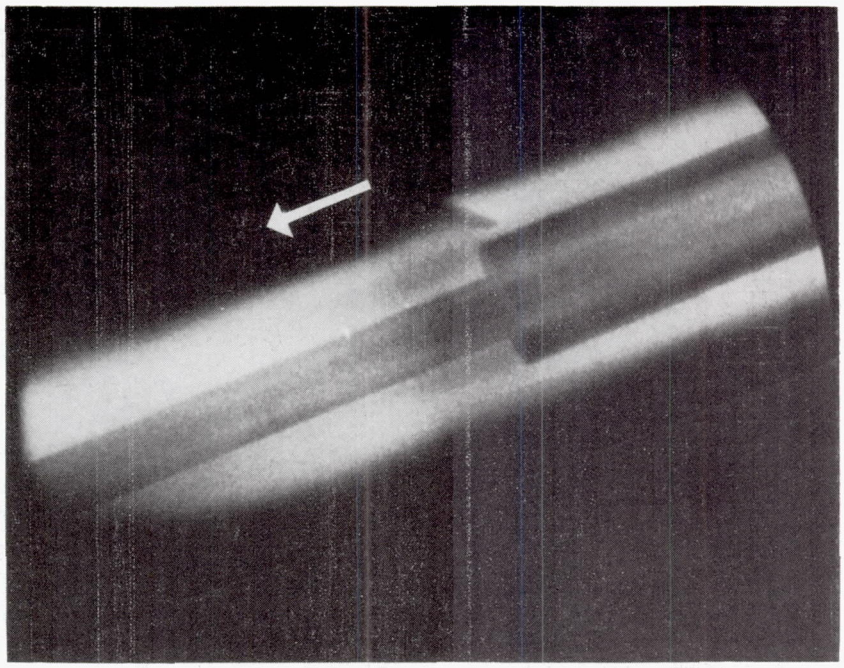

Frame 3 (time interval, 0.003 sec; camera speed, 1310 frames/sec.)

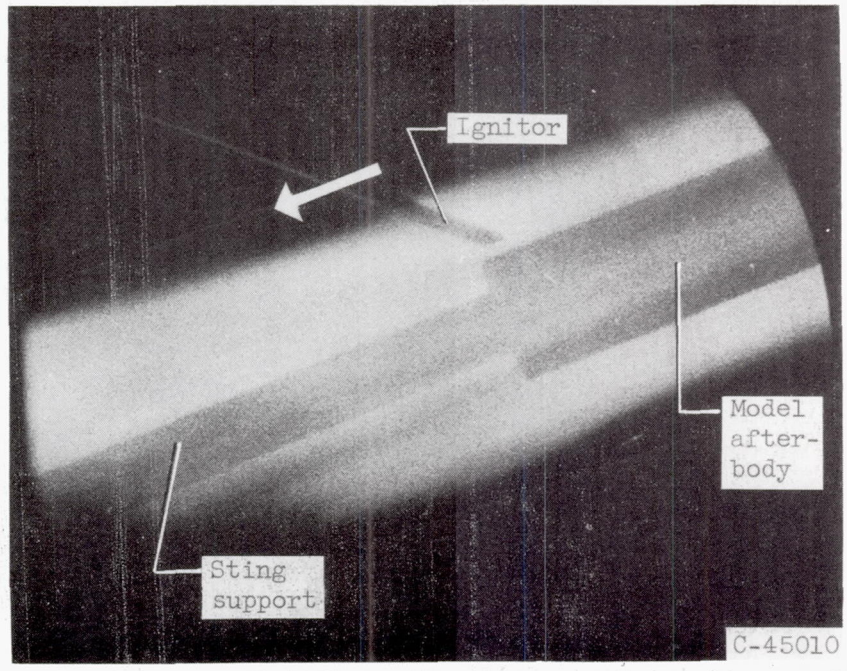

Frame 4 (time interval, 0.008 sec; camera speed, 1310 frames/sec.)

(a) Continued. Directly-photographed motion-picture frames.

Figure 17. - Continued. Single motion-picture frames of run 3 showing the development from ignition of a typical good combustion run.

4139

CJ-6 back

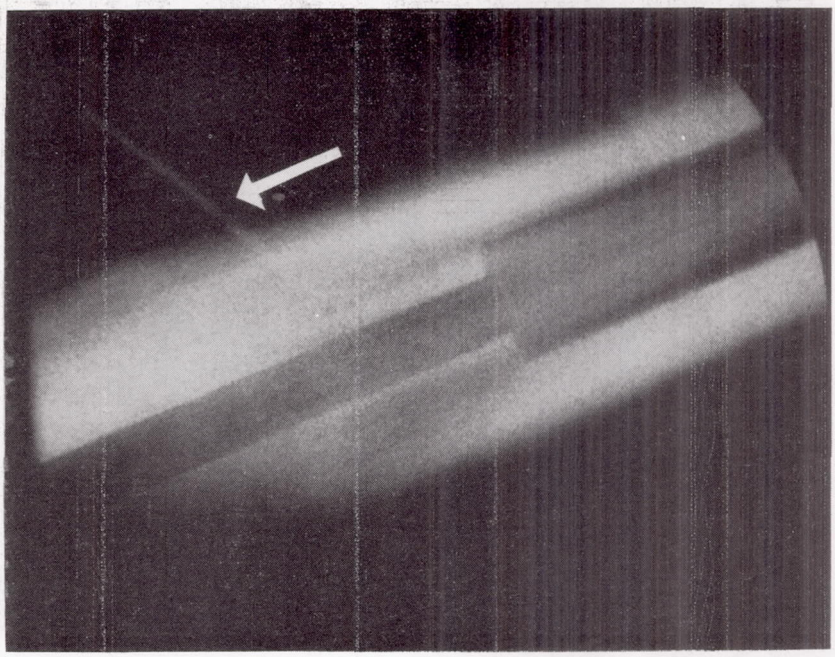

Frame 5 (time interval, 0.135 sec; camera speed, 1380 frames/sec.)

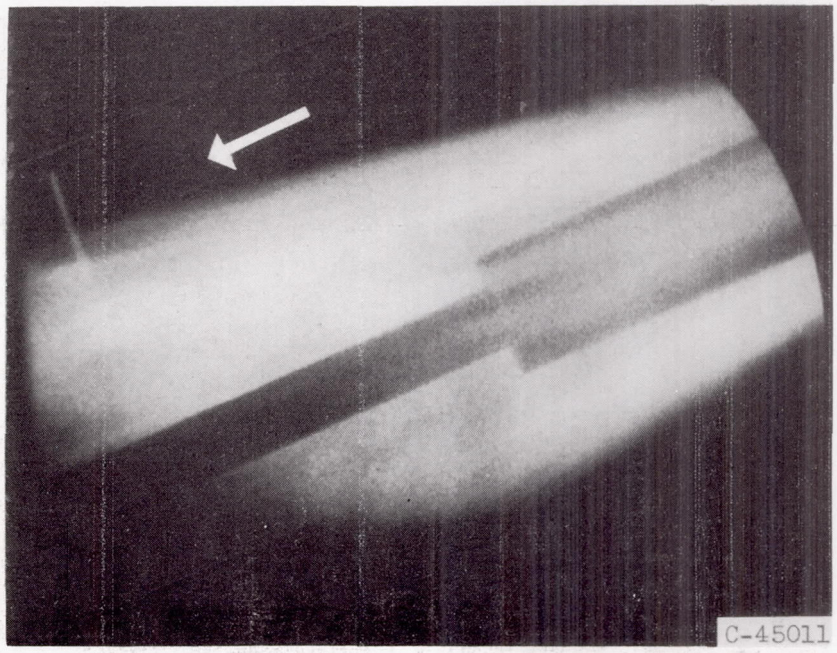

Frame 6 (time interval, 0.158 sec; camera speed, 1420 frames/sec.)

(a) Continued. Directly-photographed motion-picture frames.

Figure 17. - Continued. Single motion-picture frames of run 3 showing the development from ignition of a typical good combustion run.

4139

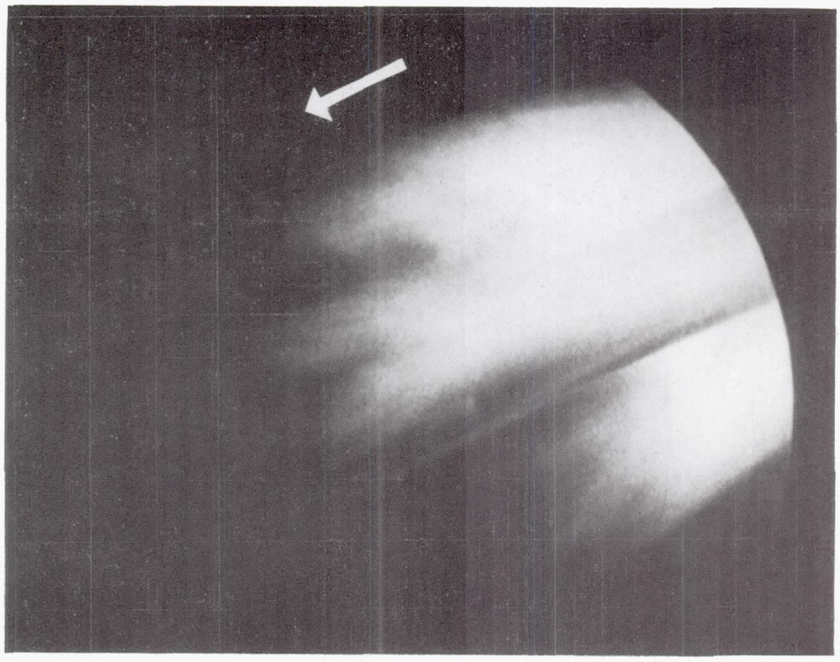

Frame 7 (time interval, 0.170 sec; camera speed, 1420 frames/sec.)

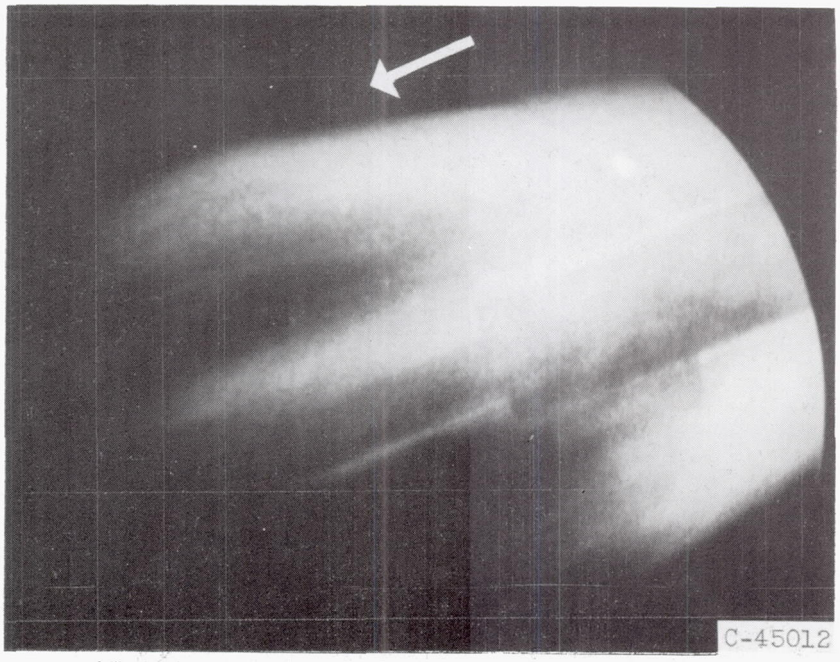

Frame 8 (time interval, 0.179 sec; camera speed, 1420 frames/sec.)

(a) Concluded. Directly-photographed motion-picture frames.

Figure 17. - Continued. Single motion-picture frames of run 3 showing the development from ignition of a typical good combustion run.

4139

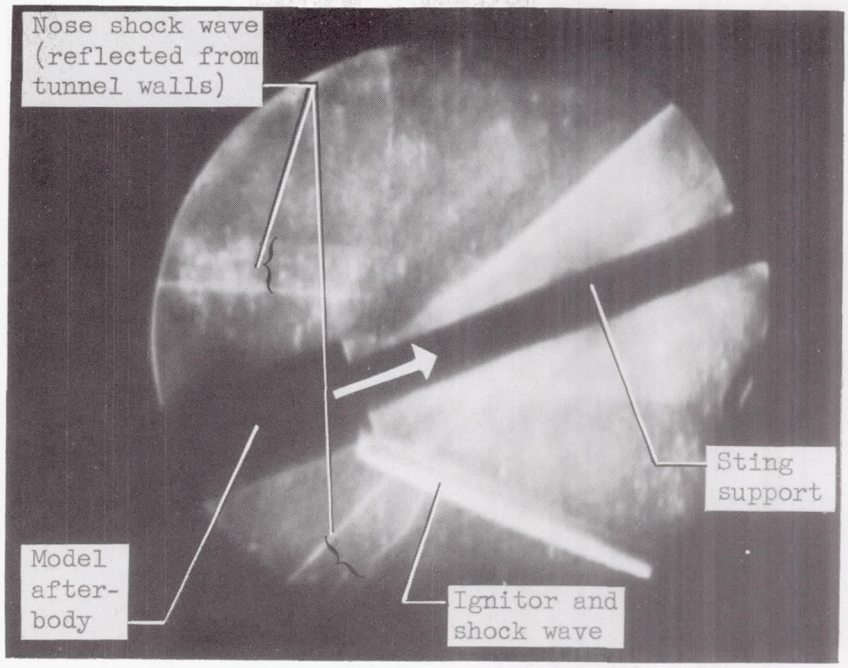

Frame 1 (prior to ignition)

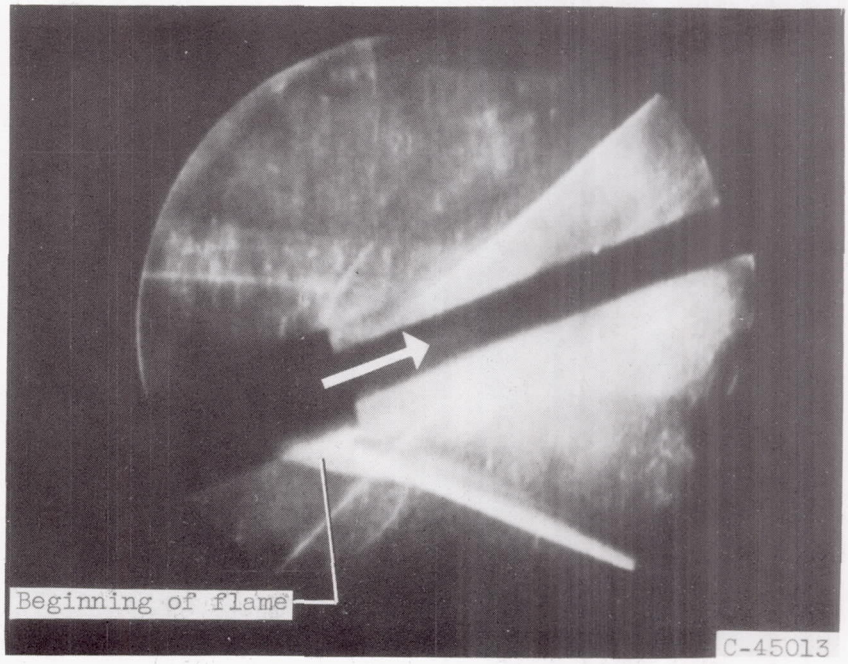

Frame 2 (time interval, 0 sec.)

(b) Schlieren motion-picture frames, camera speed 1560 frames per second.

Figure 17. - Continued. Single motion-picture frames of run 3 showing the development from ignition of a typical good combustion run.

4139

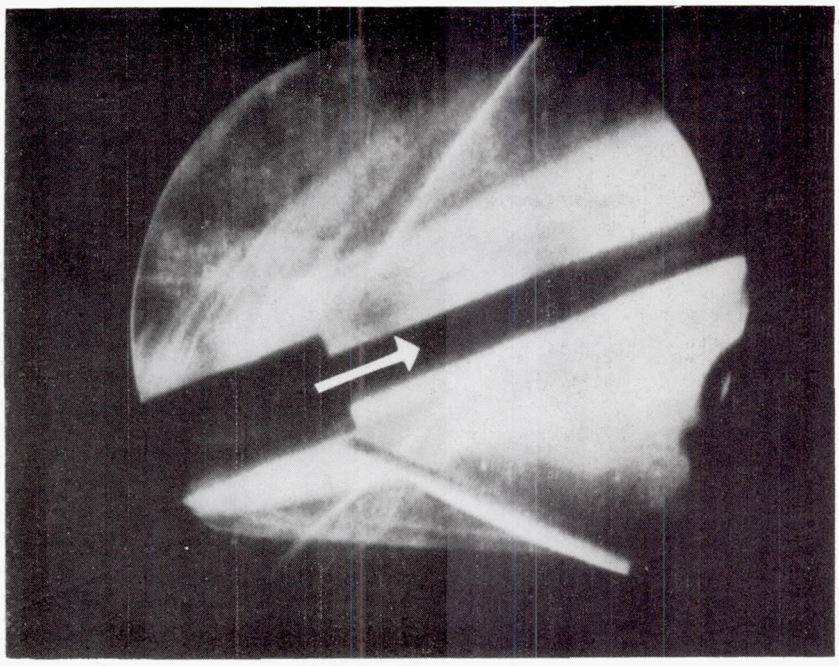

Frame 3 (time interval, 0.001 sec.)

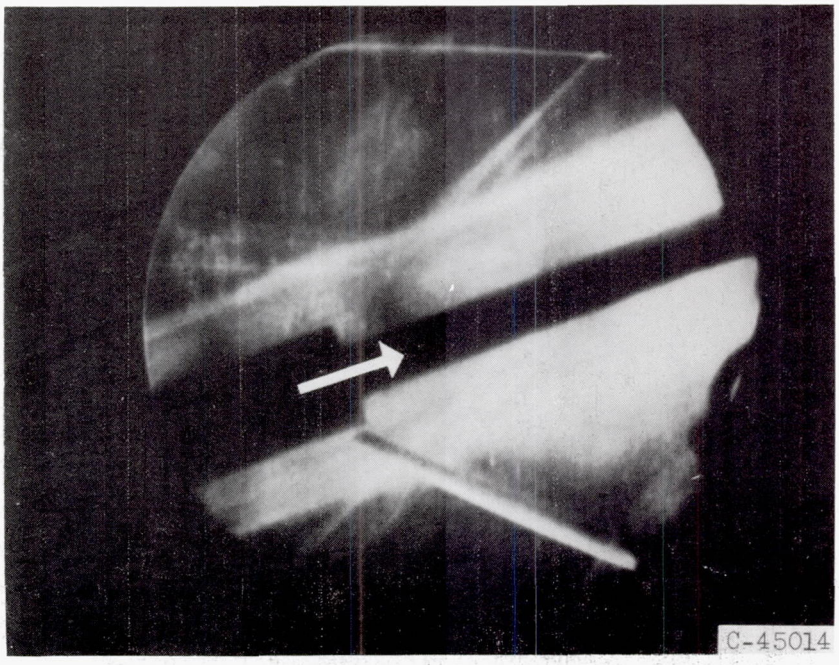

Frame 4 (time interval, 0.002 sec.)

(b) Continued. Schlieren motion-picture frames, camera speed 1560 frames per second.

Figure 17. - Continued. Single motion-picture frames of run 3 showing the development from ignition of a typical good combustion run.

4139

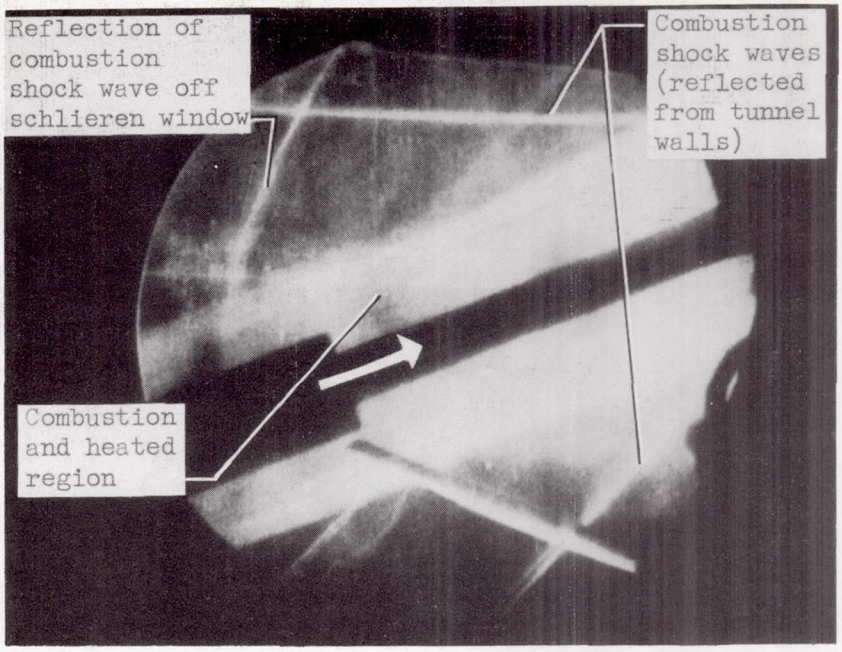

Frame 5 (time interval, 0.003 sec.)

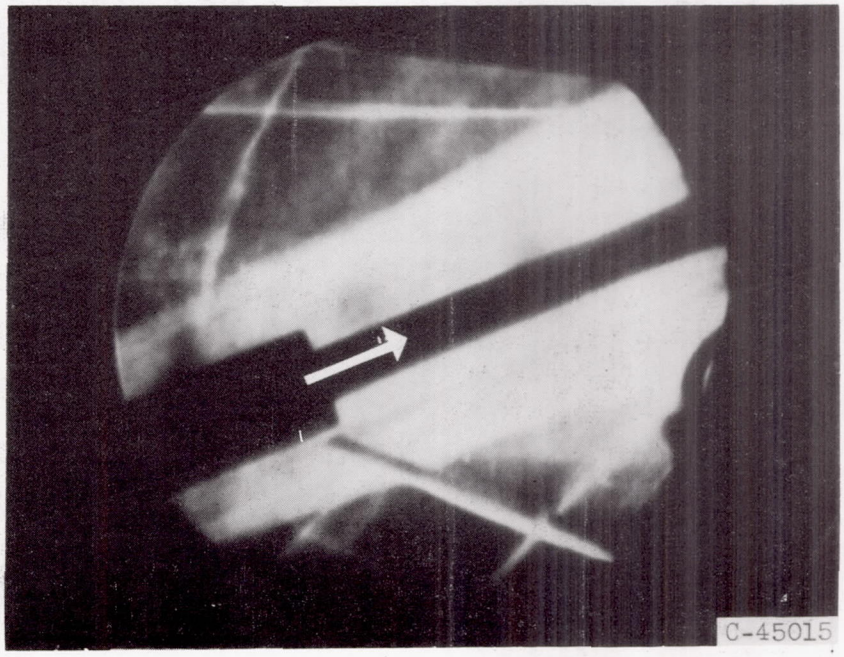

Frame 6 (time interval, 0.106 sec.)

(b) Continued. Schlieren motion-picture frames, camera speed 1560 frames per second.

Figure 17. - Continued. Single motion-picture frames of run 3 showing the development from ignition of a typical good combustion run.

4139

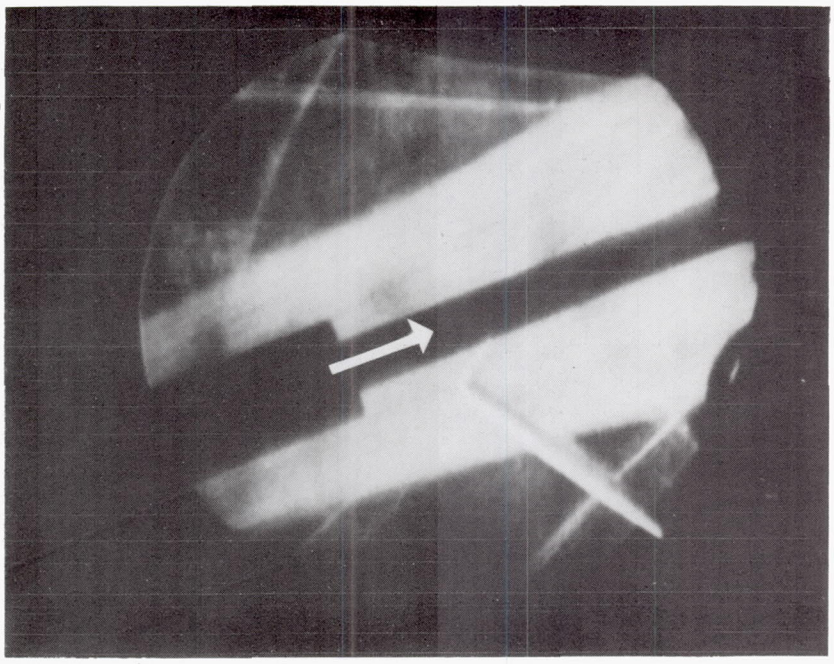

Frame 7 (time interval, 0.134 sec.)

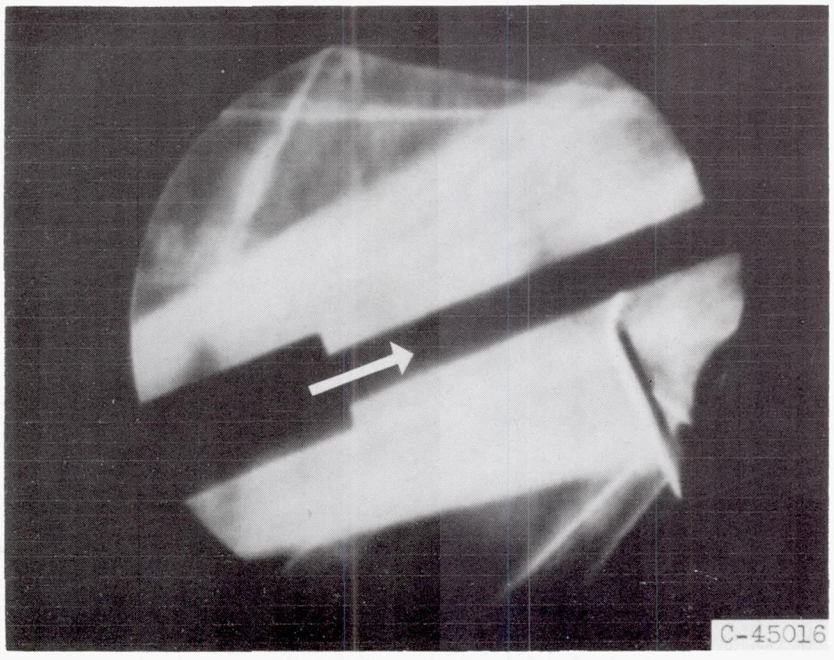

Frame 8 (time interval, 0.158 sec.)

(b) Continued. Schlieren motion-picture frames, camera speed 1560 frames per second.

Figure 17. - Continued. Single motion-picture frames of run 3 showing the development from ignition of a typical good combustion run.

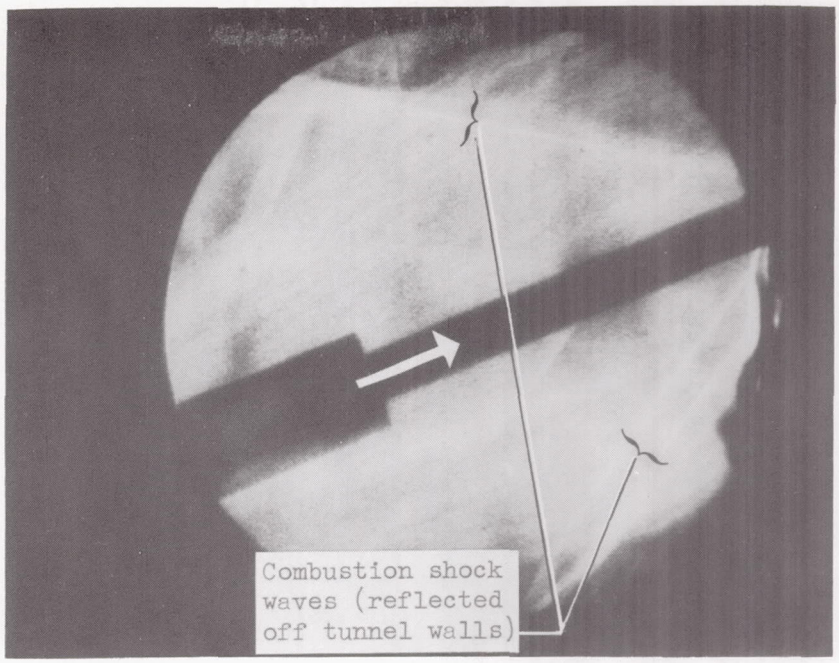

Frame 9 (time interval, 0.169 sec.)

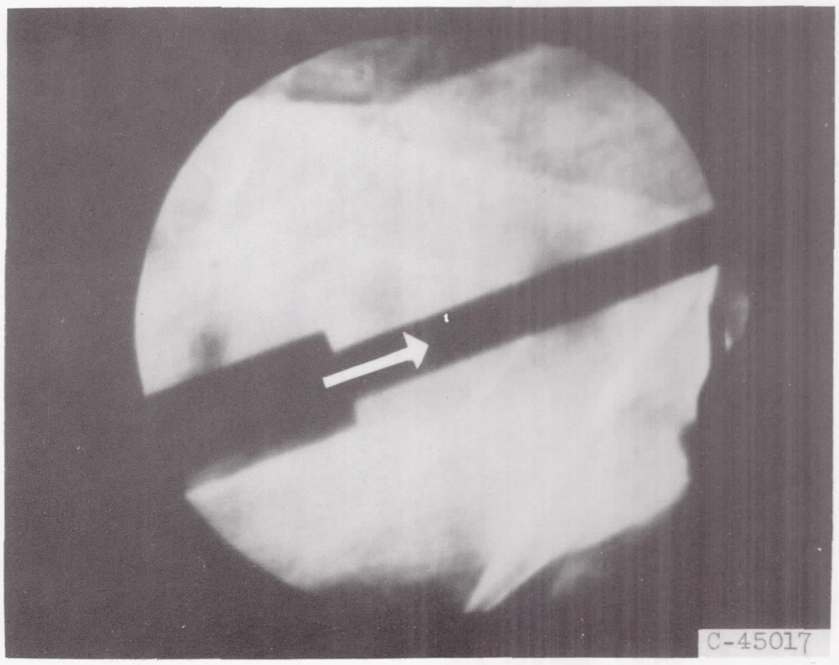

Frame 10 (time interval, 0.178 sec.)

(b) Concluded. Schlieren motion-picture frames; camera speed, 1560 frames per second.

Figure 17. - Concluded. Single motion-picture frames of run 3 showing the development from ignition of a typical good combustion run.